Thermite-for-demise (T4D): Experiments and numerical modelling on ball-bearing unit mock-ups containing thermite in an arc-heated wind tunnel

A. Finazzi [a,1], D. Daub [b,2], F. Maggi [a,*,3], C. Paravan [a,4], S. Dossi [c,5], T. Lips [d,6], G. Smet [e,7], K. Bodjona [e,7]

[a] Politecnico di Milano, Milano, MI, 20156, Italy
[b] Deutsches Zentrum für Luft- und Raumfahrt e.V. (DLR), Köln, 51147, Germany
[c] ReActive Powder Technology s.r.l., Milano, MI, 20123, Italy
[d] HTG - Hyperschall Technologie Göttingen GmbH, Bovenden, 37120, Germany
[e] European Space Agency - ESA/ESTEC, Noordwijk, 2200, AG, the Netherlands

ARTICLE INFO

ABSTRACT

The use of thermite to aid spacecraft demise during atmospheric re-entry has been investigated in the ESA-TRP SPADEXO project. An experimental campaign in DLR's L2K arc-heated wind tunnel facility was dedicated to explore the Thermite-for-Demise concept. Steel mock-ups of a ball bearing unit, partially filled with thermite, were placed in L2K. The breadboards were then exposed to an air flux simulating the typical conditions that characterize spacecraft re-entry. In this paper, the key results of the tests are presented. The dispersion of a mechanically activated fraction of thermite proved to be effective in controlling the overall charge ignition temperature. Thermite-induced demise was experimentally verified in the wind tunnel. The SCARAB software was extended and used to rebuild the retrieved thermal data. The results of the simulations were in good agreement in both predicting the ignition timing and the effects of the thermite charge on the sample.

1. Introduction

The growing number of space debris and non-manoeuvrable satellites orbiting around Earth is a serious threat to the safe access and use of the outer space. The severity of this problem is evidenced by the number of international organizations calling for action. The last document issued on this topic is the Zero Debris Charter [1], unveiled by the European Space Agency (ESA) at the 2023 Space Summit in Seville, Spain. More than 40 organizations collaborated on its final version. Despite the document being non-binding, it traces out future concerted directions of improvement such as the limitation of the mission's probability to

generate space debris, which should not exceed 1 in 10000, and the reliability of the post-mission disposal (PMD), that should reach a success probability of 99 %. The Zero Debris Charter is not the only document calling for more stringent rules to mitigate space debris. Another recent example is the reconsideration of the 25-year rule proposed by the Council of the European Union [2]. The US Federal Communications Commission (FCC) has already acted in this sense, tightening the requirement to a maximum of 5 years [3].

Even if the solicitation for tighter mitigation rules is commendable, it is not the only aspect of the problem to be considered. Both the ESA's Annual Space Environment Report [4] and the Inter-Agency Space

Debris Coordination Committee (IADC) Report on the Status of the Space Debris Environment [5] show that global space activity is only partially compliant with current mitigation rules. In the next 25 years, the space debris population could double if the compliance level with the IADC guidelines is not improved. Moreover, the number of space junk objects could multiply up to 10 times due to the increase of catastrophic collision events. In this frame, a particularly critical situation is the one of the Low Earth Orbit (LEO). The space traffic in this region is now 10 times the level observed in the year 2000. For these protected orbits, the main mitigation measure is the atmospheric re-entry at the end-of-life (EOL). In this respect, both the aforementioned reports highlight how a large share of satellites does not respect the 25-years rule. If the naturally compliant ones are not considered, no more than 50 % of the EOL maneuvers is successful. If this percentage is compared to the minimum compliance threshold required (90 % [6,7]) and to the one proposed by the Zero Debris Charter (99 % [1]), it is evident how the global space activity is still far from the requested levels.

The need to increase the share of spacecraft successfully re-entering on ground could imply problems for our society. Indeed, each re-entry is associated to a casualty risk, which is a measure to quantify the probability to harm people or damage goods at the end of the re-entry process. A first strategy to avoid this risk is to perform a high-thrust maneuver at the spacecraft's end-of-life, targeting an uninhabited area. Unfortunately, this solution implies a significant impact on the mission's budget and complexity. A second option is to let the spacecraft re-enter in the Earth's atmosphere in an uncontrolled way, if the casualty risk on ground is considered as low as needed. For example, the acceptability threshold for ESA projects is currently 1 in 10000 [8]. Then, it is important to adopt specific design solutions to limit the casualty risk on ground if one wants to exploit the advantages of an uncontrolled re-entry. The Design-for-Demise (D4D) approach follows this rationale. D4D is the intentional design of the spacecraft to comply with the casualty risk limits, aiming at enlarging the share of spacecraft that can access an uncontrolled re-entry. Among the benefits of this end-of-life solution are the reduction of the mass needed on board, considering both the propellant and the propulsion system, and the potential simplification of the spacecraft design.

The possible D4D approaches are different and several papers have been published in the recent years to evaluate them [9–11]. A first technique aims to reduce the area of casualties on the ground, by containing the fragments using nets or tethers. A second strategy consists in limiting the mass of the spacecraft surviving the re-entry process. In this frame, the use of more demisable materials in lieu of titanium or steel, the weakening of structural joints to provoke early fragmentation, or the use of particular shapes to control the heat load distribution are among the techniques that have been proposed. A relatively new approach in the same direction is the maximization of the available heat by incorporating reactive materials in the structural voids of particularly robust components [12–14]. Following this paradigm, energetic materials with high adiabatic flame temperature and high energetic density become of paramount interest. Thermites are good candidates for this role, thanks to their characteristics [15].

This last technology, hereby named Thermite-for-Demise (T4D), is the focus of this paper. The use of thermites to aid spacecraft demise during re-entry has been studied in the framework of the ESA-TRP SPADEXO project. Hyperschall Technologie Göttingen GmbH (HTG) led the activity, which involved Politecnico di Milano, DLR-Cologne, Reactive Powder Technology s.r.l., and Airbus Defence and Space. Thermite charges were embedded in simple-shaped ball bearing unit mock-ups and these samples were tested in DLR's L2K arc-heated wind tunnel to verify the effectiveness of this technique. The acquired data were then compared with the numerical description provided by a specifically developed software package. In the following sections, key results for two different geometries are reported. Section 2 outlines the background of the study, focusing on guidelines for D4D verification and thermite characteristics. In Section 3, the mock-ups and the thermite

charges that have been placed in the wind tunnel are detailed. Section 4 presents the characteristics of the experimental facility and of the numerical model. In Section 5 the obtained results are discussed. The conclusions and next steps for the investigation on T4D are outlined in Section 6. Finally, Appendix A reports the complete dataset of the experimental campaign and of the numerical simulation.

2. Background

2.1. D4D technology verification

The verification of a D4D strategy is a difficult task. Tests in operative conditions are complex and expensive. Even assuming unlimited budget, problems such as the communications blackouts experienced by a re-entering spacecraft are hard to overcome. This is the reason why to this day no destructive re-entry experiments aimed at measuring the break-up of a spacecraft in space environment were performed. ESA's DRACO (Destructive Re-entry Assessment Container Object) project, to be launched in 2027, will be the first of this kind [16]. Until now, the observation from the ground of re-entry events has been able to provide the scientific community only limited information (e.g., the typical altitude of the main fragmentation event [17]). Therefore, for now the verification of D4D technology needs to rely heavily on ground testing and numerical simulations. To support research on this topic, ESA established guidelines and best practices to assist in the verification of D4D at the material, equipment and system levels [18].

The first step of an experimental campaign to verify a D4D technology is the selection of an appropriate facility. This choice must be guided by the purpose of the investigation. If the objective is to characterize the material properties or the thermochemical behavior of the sample surface, static tests in vacuum chambers heating up the equipment to temperature relevant to a re-entry condition are typically performed. These facilities can sometimes even apply prescribed mechanical loads on the sample to determine their influence, but the interactions with a high velocity flow, representative of a re-entry condition, are excluded. Shock tubes are a second type of facility that can be used for D4D verification. These instruments are of particular interest if the aerodynamic conditions (Mach and Reynolds number) of a re-entry process are desired. As the test time is limited to fractions of seconds [19], it is not possible to reproduce the heat loads of an atmospheric re-entry. Nevertheless, these tests can be useful to study the aerodynamics and the shock interactions. A third possibility is represented by high-enthalpy hypersonic wind tunnels. A continuous high-enthalpy flow is created and directed through a nozzle on the sample under study. The method in which the high-enthalpy flow is generated categorizes the wind tunnel and defines the phases of the re-entry process that can be recreated. Among these facilities, the arc-heated wind tunnels are able to produce particularly high heat loads; therefore, they are indicated to study the late phase of a re-entry. The dimensions of the test chambers are typically limited, hence it is common to conduct the investigation at equipment or material level. In Europe, the largest test chamber is the one of CIRA's SCIROCCO test facility (<2 m) [20]. The ordinary sample size that can be placed in these premises is below 0.5 m. The main limitations of these wind tunnels are the difficulties to reproduce the tumbling motion and the dynamic heat load condition of a re-entering spacecraft. Therefore, it is common to keep the sample at a fixed orientation and to select a single level of heat flux that is then maintained constant during the test. Nevertheless, these experiments are vital to tune re-entry numerical models.

The other tool used in the verification of a D4D technology is numerical analysis. Several software packages have been proposed over the years, each with a different level of detail and specific qualities. The baseline in Europe is ESA's Debris Risk Assessment and Mitigation Analysis (DRAMA) [21], provided by the Agency to the industries to verify the compliance of their products to the space debris mitigation guidelines. In general, re-entry numerical packages can be classified

depending on their level of detail. Lumped mass models can give a first indication of what can be expected (e.g., the TRANSatmospheric SImulation Tool, TRANSIT [22]), while more sophisticated tools can simulate the re-entry with higher level of detail (e.g., the Spacecraft Aerothermal Model (SAM) [24], or PAMPERO [25]). Among the other European numerical models, the Spacecraft Atmospheric Re-entry and Aerothermal Breakup (SCARAB) [26] is of primary relevance and is one of most detailed ones. SCARAB was developed under the lead of HTG in the framework of ESA/ESOC contracts since 1995. It is a comprehensive tool that simulates flight dynamics, aerodynamics, aerothermodynamics, thermal and structural analysis. The comparison to other re-entry tools and the validation with in-flight measurements and observation proved its capabilities. Even if its primary commercial aim is the estimate of the casualty risk of a re-entry process, it has been used successfully to investigate D4D technologies in hypersonic wind tunnels. For this purpose, a dedicated simulation environment named Wind Tunnel Mode (WTM) was developed. SCARAB WTM was already used to describe experiments in DLR's L2K and L3K in past projects. A first example is the Characterization of Demisable Materials (CHARDEM) activity [27], which involved the characterization of five different materials commonly employed by the space industry. The results of this analysis were of paramount importance for the establishment of ESA's material database ESTIMATE [28]. Another study carried out with the use of SCARAB WTM to rebuild L2K data is the ESA-founded ERASD test campaign [29], which is of particular relevance for the investigation presented in this paper. A realistic Ball Bearing Unit (BBU) geometry was filled with thermite and placed in the high-enthalpy hypersonic wind tunnel to prove the T4D concept. The results of these experiments were the basis of the SPADEXO project.

2.2. Thermites

Thermites characteristics are particularly attractive to aid spacecraft demise exploiting exothermic reactions. This class of pyrotechnic materials has a high adiabatic flame temperature and high energetic density. Moreover, their relative insensitiveness to external stimuli with respect to other energetic materials can grant safe operations if they are managed properly. These materials, usually in the form of powders, can release a noticeable amount of heat upon reaction. They are formed by a metal and a metal oxide which, if ignited, start a redox reaction that results in the oxidation of the starting metal and in the reduction of the starting oxide. H. Goldschmidt patented this process in 1895 to produce pure metals. In the following decades, thermites were used in a variety of applications: rail welding [30], cutting torches [31,32], green firecrackers [33], and incendiary grenades [34] are some examples. The main reason for such a wide field of application lies in their tunability. The selection of the metal - metal oxide couple leads to mixtures with very different properties (e.g., heat generated, gas production, and sensitivity [15]). Moreover, it is possible to act on other characteristics to obtain fine-tuning of the reaction: granulometry, particle shape, oxidizer to fuel ratio, and compaction influence the reaction rate and the reactivity of the mixture. The material preparation process is also of paramount importance. A particular process that can be applied to a powder mix to alter its features is activation. This family of procedures can involve the modification of the shape, surface finish, composition, or structure of the particles to modify the reactivity. Activation can be purely mechanical, purely chemical or mechanochemical. These methods are extensively discussed in Refs. [35,36]. In the SPADEXO project, mechanical activation through high-energy ball milling was used to increase the reactivity of a portion of the starting powder to guarantee reliable ignition even at temperatures considerably lower than the ignition temperature of the starting thermite. In these experiments, the pyrotechnic charge was enclosed in the sample geometry and heated by the high-enthalpy flow of the wind tunnel, which eventually triggered the passive ignition of the energetic material. In this configuration, the expected dominant heat transfer mode between the reacting

thermite and its vessel is heat conduction. The ideal properties of the formulation are a high energetic density to be effective even if enclosed in limited structural voids, a high adiabatic flame temperature to grant effective heat transfer to the containment vessel, low gas generation to prevent uncontrolled fragmentation, relative insensitivity to avoid unintended ignition, and tunable reactivity to select the re-entry phase in which the charge should ignite.

3. Materials tested

3.1. Equipment mock-ups

Two simple geometries were placed in the L2K wind tunnel to test the T4D concept. As suggested by the results of the ERASD project [29], simplified mock-ups were preferred to more realistic configurations both to study the fundamental mechanisms of the experiments and to ease their numerical rebuilding. Therefore, two geometries were derived from a Ball Bearing Unit (BBU) excluding details such as ball bearings and the layered structure of the oil chamber. Figs. 1 and 2 show the two configurations, that differ only for the thickness of the lateral wall. For this reason, the two geometries will be respectively referred to as thick-walled BBU and thin-walled BBU. Both BBU mock-ups had an external diameter of 50 mm.

The whole set of samples was made of steel 316L. Five type K class 1 thermocouples were placed in each sample as shown in Fig. 3. All the thermocouples were centered with respect to the internal volume except for the one inside the thermite. This last one was only centered in the middle of the sample in the tests at full filling. In all other thick-walled BBU tests, the thermocouple was placed 8 mm from the lateral wall and slightly upstream with respect to the center of the cavity, at 12.7 mm from the center line. In all tests involving the thin-walled BBU, this thermocouple was placed again at 8 mm from the lateral wall, but 18.3 mm upstream with respect to the center line. In the reference runs without thermite, this thermocouple was absent. Furthermore, two pyrometers (Maurer KTRD 1485 and QKTRD 1483) registered the temperature of the center of the front face. Two IR thermocameras (Optris PI 1 M and Infratec VarioCAM HD) acquired further thermal data. Finally, videos of the tests were recorded from different points of view.

A specific feature of the mock-ups is the safety lid that closes the top of the geometry. This design was adopted to limit the pressure build-up inside the samples, to avoid potential damage to the facility. In all tests involving thermite, except for the first run at full filling, the lid was equipped with venting holes and kept in place by two tantalum wires.

3.2. Thermite charge

The thermite selection process for the SPADEXO experimental campaign resulted in the choice of an aluminum - hematite (iron oxide) formulation. This composition is the most widely used in terrestrial applications and has been broadly characterized over the decades. Its reaction can be described as per Eq. (1)

$$2Al + Fe_2O_3 \rightarrow Al_2O_3 + 2Fe + \Delta H \tag{1}$$

Thermochemical computations can provide some information about the thermite reaction. Its theoretical heat release in stoichiometric reaction ΔH is equal to 3958.20 kJ/kg, its adiabatic flame temperature is 3135 K, and in adiabatic conditions the 7.84 % in mass of its products gasifies. The characteristics of the starting aluminum and iron oxide powders are shown in Table 1. In some tests, a fraction of the thermite charge has been mechanically activated through high-energy ball milling to lower its temperature of ignition. Various integration methods of the activated fraction in the main charge were explored during the experimental campaign. The first strategy adopted was the placement of the activated thermite in the core of the reactive charge. This layout replicates the one tested in small scale at Politecnico di Milano, that
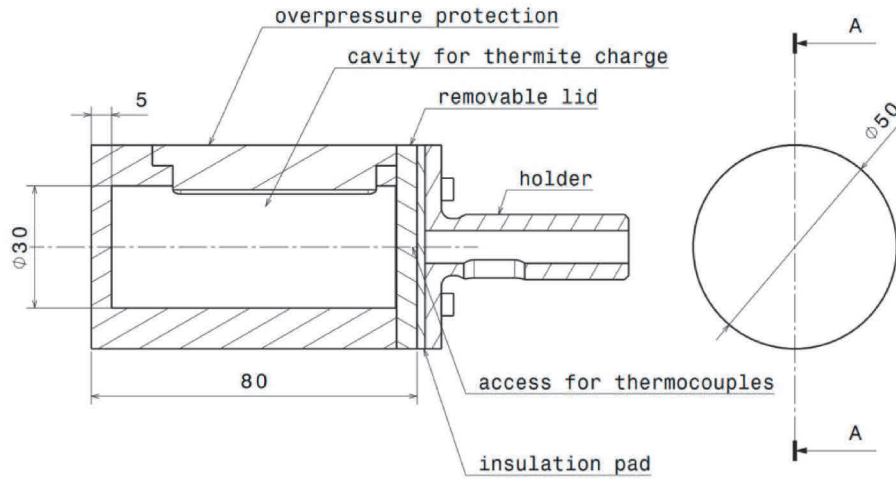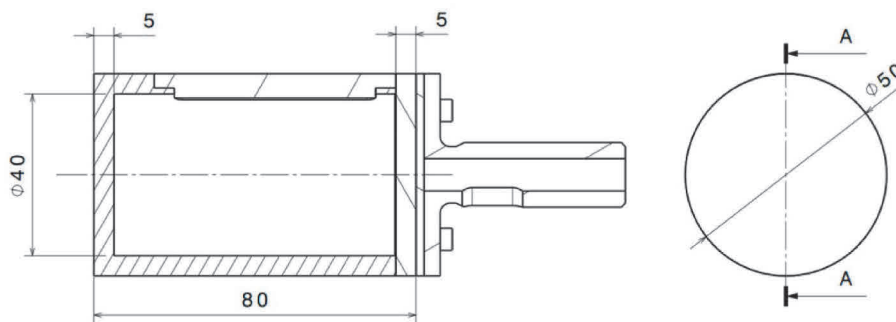
Fig. 1. Thick-walled BBU geometry.

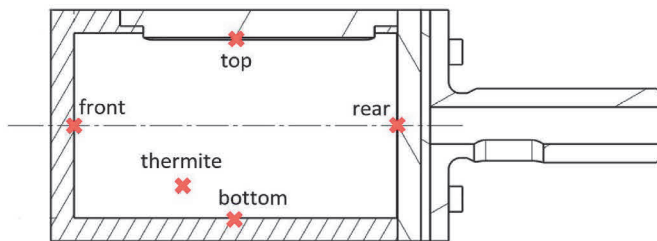
Fig. 2. Thin-walled BBU geometry.

Fig. 3. Typical thermocouple positions in the BBU mock-ups (not in scale).

Table 1
Characteristics of the starting powders.

Material	Characteristics
Al	Sperical, 30 μm
Fe_2O_3	−325mesh (≤44 μm)

Fig. 4. Thick-walled BBU sample partially filled with Al + Fe_2O_3 thermite.

proved to be reliable and effective in controlling the temperature of ignition of the overall charge for thermite masses between 1 and 3 g. A second solution was the mechanical mixing of loose activated and loose standard powder, creating a uniform blend. The last option consisted in randomly distributing some activated pellets in the loose standard thermite. The energetic material was placed in the central void of the samples, as shown in Fig. 4. The production, activation, and pelletization of the thermite was performed by ReActive Powder Technology s.r. l. Table 2 presents all the tests that will be analyzed in this paper, indicating geometry, thermite charge, heat flux level in the wind tunnel,

and other comments. Tests 2 and 3 are the only ones performed at full filling, using a vibration plate to reach the tap density of the powder.

4. Methodologies

4.1. Arc-heated wind tunnel

The facility used to conduct the experimental campaign was DLR-

Table 2

Test matrix. Please notice that ''P'' stands for activated pellets, ''A'' for activated loose powder, and ''T'' for standard loose thermite.

TestID	Geometry	Filling	Thermite charge [g]	Comments
1	Thick-walled	None	–	–
2	Thick-walled	100 %	4.9P + 7.0A + 54.3T	Central core of P and A
3	Thick-walled	100 %	4.1P + 5.3A + 53.0T	Central core of P and A
4	Thin-walled	None	–	–
5	Thick-walled	50 %	29.0T	–
6	Thin-walled	26 %	29.1T	–
7	Thick-walled	50 %	4.7A + 24.5T	Loose blend
8	Thick-walled	50 %	4.7P + 24.4T	Randomly distributed pellets
9	Thin-walled	26 %	9.2A + 19.7T	Loose blend
10	Thin-walled	26 %	9.3P + 19.8T	Randomly distributed pellets
11	Thin-walled	26 %	29.1T	Higher heat flux
12	Thin-walled	39 %	44.9T	–
13	Thin-walled	52 %	58.2T	–

Cologne's L2K (Fig. 5). This premise is an arc-heated wind tunnel (WT). As this category of WT can produce particularly high heat loads, it is suitable to investigate the last phase of an atmospheric re-entry. One of the objectives of the study was to explore the passive ignition of the thermite charge as a result of the heat provided by the interaction of the spacecraft with the atmosphere. Passive ignition of the thermite is desired to occur at relatively high temperatures to avoid potential unintended ignition. The L2K uses a Huels-type arc-heater with a maximum electrical power of 1.4 MW and can reach cold wall heat fluxes of up to 3.0 MW/m^2 at stagnation pressures up to 250 hPa. Hypersonic free-stream velocities are reached thanks to a convergent-divergent nozzle. The nozzle's expansion part is conical with a half angle of 12°. Various throat diameters can be combined with different nozzle exit diameters to provide the necessary flexibility. Moreover, it is possible to vary the test gas to replicate the conditions of the atmosphere of other planets (e.g., Mars). An extensive discussion of its characteristics and of the type of studies conducted in this facility can be found in Ref. [37]. In the SPADEXO campaign, the nozzle was set up with a 29 mm nozzle throat and a 200 mm wide exit. The samples were placed at 120 mm from the nozzle. The working gas was air. For the tests

discussed in this paper, the tunnel conditions resulted in a reference cold wall heat flux of 750 kW/m^2 for all the samples except Test 11, in which a reference cold wall heat flux of 800 kW/m^2 was used.

4.2. Numerical analysis

The numerical model used to rebuild the data obtained during the experimental campaign was SCARAB 3.1L in its Wind Tunnel Mode (WTM). A package specifically developed to simulate the heat released by the thermite upon ignition was integrated into the software. The pyrotechnic charge was represented as an internal heat source, triggered once the vessel temperature overcame the ignition temperature of the powder at least in one point. This approach was preferred to the introduction of a dedicated thermite primitive for its simplicity and its inherent consistency with SCARAB representation of spacecraft. However, the absence of a dedicated primitive implied that the thermite was not able to contribute to the overall mass and thermal inertia of the system. To overcome this limit, its presence was accounted for modifying the mass and the specific heat of its vessel. A method to deactivate the thermal inertia of the thermite was introduced in the model, as it was not possible to determine a-priori if this contribution was helpful or not to the test rebuilding. The thermite apparent density was computed considering a known thermite volume and its weight, measured with a scale before the experimental campaign. The thermite density was assumed constant during the simulations. Its specific heat was considered temperature dependent and calculated starting from the NIST-JANAF tables [38], considering the relative weight of the species in the formulation. The reaction was considered one-step, happening at the temperature chosen by the user and derived from experiments. For this reason, before the ignition temperature the specific heat of the energetic material was computed considering the reactant species, while for higher temperatures the charge was considered to be completely composed by reaction products. The thermal properties of the vessel were taken from ESA's ESTIMATE [23] database. Once the reaction begins, additional heat is applied to the internal panels of the geometry. The user can select the duration and the time profile of the heat released. The application of the additional enthalpy is not stopped in case of fragmentation during the time span in which the heat release from the thermite is prescribed. Instead, the thermite continues to apply heat on the surviving fragments. This behavior is chosen because the molten thermite is expected to have at least partial residence even if the front face is demised or the top lid is opened. A variable of paramount importance for the model is the efficiency of heat transfer between the

Fig. 5. L2K measuring chamber with nozzle flange, diffuser inlet, adjustment device, and test model. The sample in the figure is not linked to the SPADEXO test campaign. Credit: DLR (CC BY-NC-ND 3.0).

reacting thermite and the surrounding vessel. For these simulations, this quantity was defined as 60 %, based on preliminary tests in non-relevant environment performed at Politecnico di Milano [22]. In the same reference, a more complete description of the thermite model is provided. To reach the best possible comparison between the experimental and numerical data, the temperature of the closest volume to the position of the real thermocouple is registered. One last remark on the numerical simulations is that the thermal gradient of the front face has also been computed. Typically, surface thickness in SCARAB is represented by a single element. For these simulations, instead, the front face was represented by a layered set of five disks, allowing to see a thermal gradient in that direction.

5. Results and discussion

The main objective of the research presented in this paper is to verify the effectiveness of an internal thermite charge in aiding the demise of its vessel in a condition that is representative of the operational environment. The adequateness of the developed numerical model needs to be verified as well. In the following sections, the experimental and numerical results are presented. Finally, the general outcomes of the campaign on the BBU-like mock-ups will be discussed, focusing on the trends that could guide future research on the topic. The temperature traces registered during the tests are presented in Appendix A, together with the numerical rebuilding obtained with the computational model. It is important to highlight that the temperature traces measured using the thermocouples cannot be considered reliable anymore after the thermite ignition. Nevertheless, their data is reported even after the first ignition event to allow the identification of secondary ignitions.

5.1. Experimental results

In the following sections, key experimental results obtained during the campaign in the L2K wind tunnel [39] are reported. Sections 5.1.1 and 5.1.2 present the objectives of the test matrix (Table 2) and the motivations for the venting holes and the random distribution of the activated thermite fraction in the standard formulation. Section 5.1.3 reports the main experimental results and the observed trend.

5.1.1. Thick-walled BBU

The tests on the thick-walled BBU geometry started with a reference run on a sample without thermite. The chosen heat flux level proved to be coherent with the desired effect on the mock-up. According to previous tests and specifications [23], melting of the samples was expected between 1650 K and 1680 K ± 10 K. The temperature recorded by the

thermocouples and the pyrometers during the test is shown in Fig. 6. The steady state temperature reached by the front face was considered high enough to potentially provoke partial demise with the use of an internal thermite charge. For this reason this heat flux level was maintained for all successive tests with the BBU geometry (except Test 11). During the reference test, the safety lid on top of the mock-up was not removed by the incoming air flow.

Then, two tests were performed on thick-walled BBU at full filling (Tests 2 and 3). In both tests, the thermite was successfully ignited. However, the pressure build-up upon thermite ignition was sufficient to remove the safety lid in both tests, even if venting holes were drilled in it before Test 3. The removal of the lid implied the loss of a significant fraction of the reactive material. Therefore, to avoid this behaviour and potential damages to the facility, in all the successive tests the quantity of thermite was reduced. Another noticeable outcome of these tests was the temperature of ignition of the charge (between 1470 and 1490 K), typical of the standard thermite in use. The integration of a core of activated thermite seemed to have no particular effect on the temperature of ignition of the overall charge. The temperature measured by the thermocouple embedded in the thermite shows that the insulating effect of the loose thermite prevents an effective heat transfer to the internal part of the charge (Fig. 7). Therefore, the temperature reached by the activated thermite core was not sufficient to provoke its ignition. As a consequence, in all successive tests the activated thermite was incorporated either in the form of randomly distributed pellets or blend of standard and activated loose thermite.

The last three tests on the thick-walled BBU geometry focused on verifying the capability of randomly distributed activated thermite to lower the temperature of ignition of the overall charge. Tests 5, 7, and 8 respectively involved a simple charge of standard thermite, a configuration with activated pellets dispersed in the main standard formulation, and a loose blend of standard and activated thermite. The thermite ignited successfully in all three configurations. The temperature of ignition of each case is reported in Section 5.1.3 along with the same result for all other tests.

5.1.2. Thin-walled BBU

The experiments focusing on the thin-walled BBU started with a reference run on a sample without thermite (Test 4). The temperature traces show a behavior similar to the one experienced for the thick-walled BBU with slightly higher heating rates. This is expected due to the reduced wall thickness.

Tests 6, 9, and 10 focused on the capability of activated thermite to control the ignition temperature of the overall charge. Test 6 involved just standard thermite, while in Test 9 a blend with loose activated
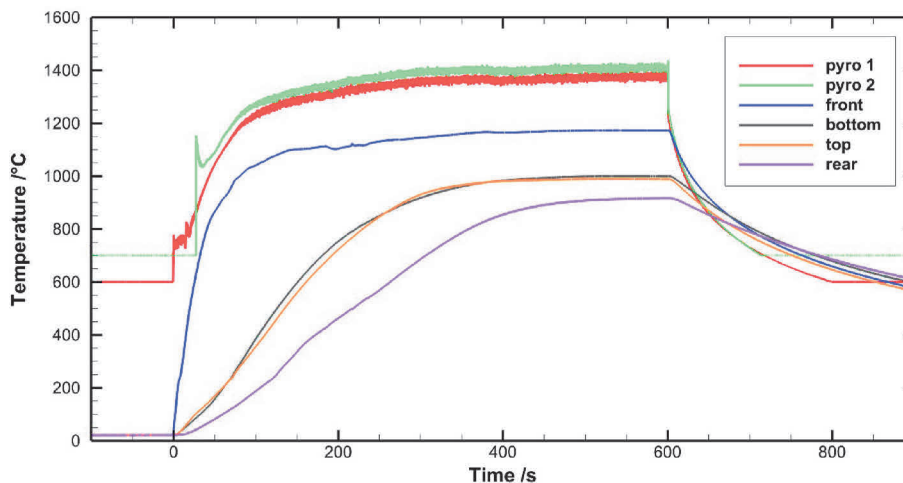

Fig. 6. Recorded temperature data during the test involving the thick-walled BBU geometry without thermite (Test 1).
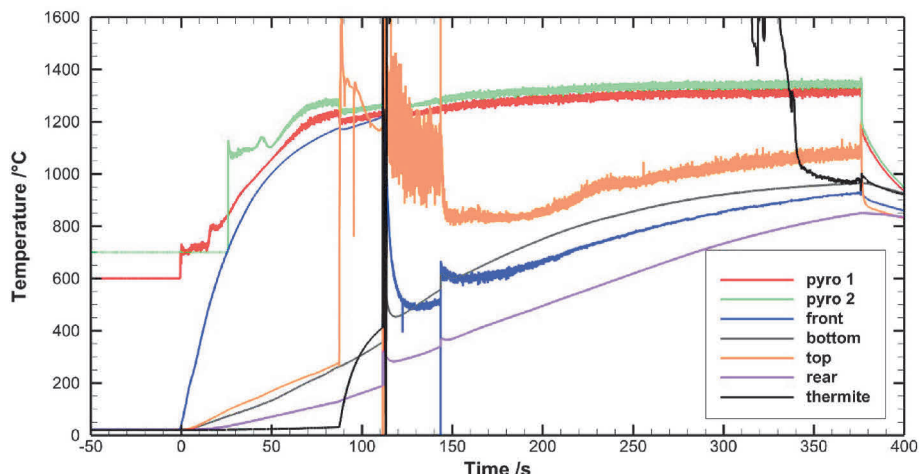
Fig. 7. Recorded temperature data during the test involving the thick-walled BBU geometry filled with thermite (Test 2).

thermite was used, and in Test 10 activated pellets were dispersed in the formulation. Note that in these tests a higher fraction of activated thermite was used in comparison to similar tests performed with the thick-walled geometry (32 % versus 16 %). The obtained ignition temperatures are presented in Section 5.1.3.

Finally, Tests 11, 12, and 13 focused on the effects that an increasing heat flux or quantity of thermite have on the demise process. All these tests involved only standard thermite. Test 11 was conducted at higher heat flux with the same thermite charge already employed in Test 6. Tests 12 and 13 were carried out with an increasing thermite mass, respectively, at 39 % and 52 % of filling.

5.1.3. Overall experimental results

The first result of the experimental campaign is the verified capability of the activated thermite to effectively tune the temperature of ignition of the main charge. The front face temperature is considered here to be the parameter of merit to characterize the reactivity of the powder, in compliance with the approach used by typical re-entry simulation tools, which focus on the external temperature of the re-entering spacecraft. Table 3 presents this value along with the activated thermite mass fraction in the overall charge. These results suggest that the primer should be placed in the proximity of the heating element to effectively control the ignition, because of the insulating effect of the standard thermite. As a matter of fact, all cases in which the charge was composed exclusively of standard thermite show an ignition

temperature between 1444 and 1557 K. The two tests at full filling, with the central core of activated thermite, fall in this range as well. As discussed in Section 5.1.1, it is suggested that the heat conduction in the charge itself was not sufficient to provide the necessary energy to the internal portion of the charge to provoke ignition. In contrast, the random distribution of loose or pelletized activated thermite powder proved to be an effective strategy to lower the ignition temperature. In this way the ignition temperature was decreased up to 450 K (from around 1500 K–1050 K). In the case of a loose blend, a higher mass fraction of activated thermite reflects in a lower ignition temperature. This is also verified for randomly distributed pellets, even to a lesser extent. Please notice that lower impact of the activated thermite mass fraction increase in the case of pellets could be caused by an unlucky distribution of pellets. The limited number of available tests is not enough to statistically quantify their impact on the overall charge ignition temperature and compare it with the loose mix solution.

A second result is that the thermite can effectively aid the demise process. In several runs, the thermites caused substantial melting, whereas nothing significant occured in the corresponding reference cases (e.g., Fig. 8). Higher thermite mass related to more pronounced melting as shown in Fig. 9. As shown in the figure, the amount of charge load was increased from Fig. 9a (without thermite) to Fig. 9d (39 % filling). The front melting progressively increased till a breach opened in the front face, for Tests 12 and 13.

Another result of the experimental campaign in the arc-heated hypersonic wind tunnel is that later ignition was associated with higher degree of demise. Fig. 10 shows the effect of two charges with different ignition temperature, using the same geometry, wind tunnel conditions, and thermite mass. Although the front face of the sample was almost intact in the test with lower temperature of ignition, substantial melting was provoked by the other thermite charge. This behavior could be due to different reasons. One possibility is that a higher pressure build-up increased the thermite fraction lost through the venting holes. The higher pressure build-up could be due to a faster reaction rate or to a higher gas generation. The comparison of the weight of the samples before and after the tests suggests this dynamic. The mass loss for three tests in which the thin-walled BBU was involved and no demise was observed is reported in Table 4. All the three tests were performed at the same filling levels, varying the fraction of activated thermite. The use of activated thermite led to a faster reaction, being more reactive than the standard thermite. This could have resulted in a steeper pressure rise that, despite the presence of the venting holes, probably reached higher values than in the case of purely standard thermite. A higher pressure level could also be the result of the presence of an excess of aluminum in the mixture, which can gasify and provoke a pressure rise. In particular, the activated thermite could be fuel rich. The activation process

Table 3

Activated thermite mass fraction and front face temperature at ignition registered during the experimental campaign. Please notice that "P″" stands for activated pellets, "A″" for activated loose powder, and "T" for standard loose thermite.

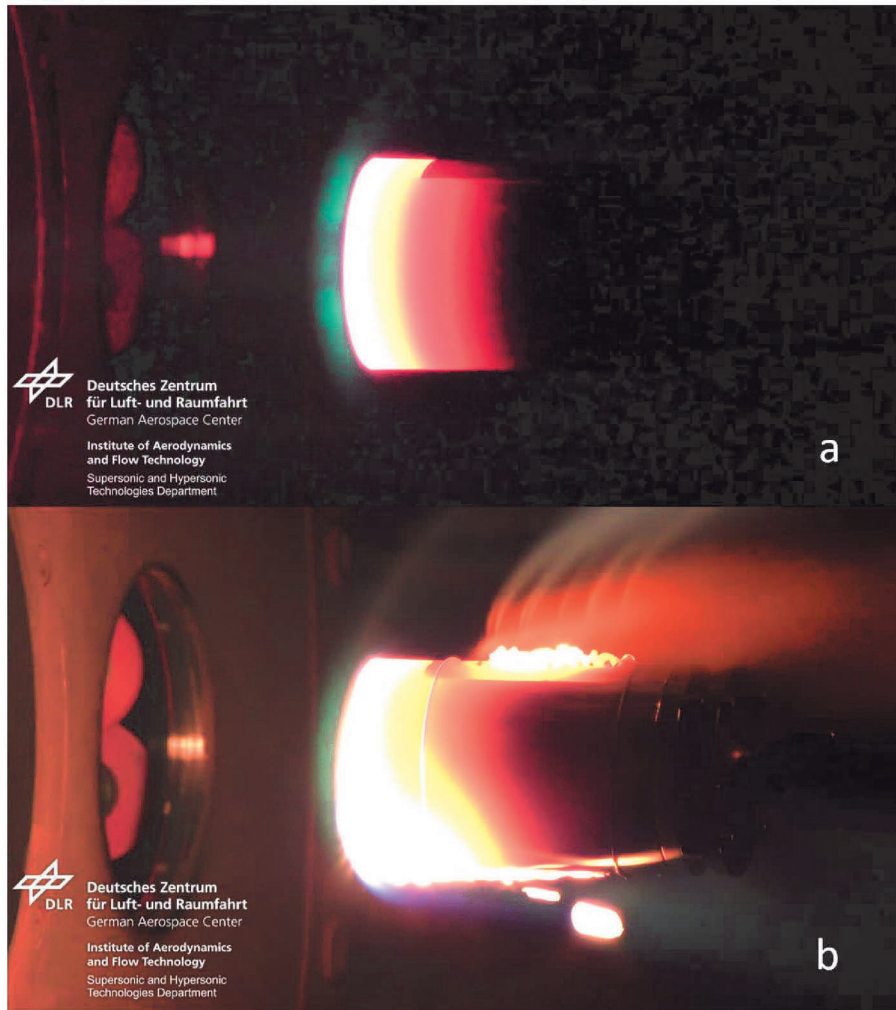| Test ID	Activated thermite fraction	Temperature of ignition [K]	Comments
1	–	–	No thermite
2	18 %	1490	Central core of P and A
3	15 %	1473	Central core of P and A
4	–	–	No thermite
5	0 %	1497	–
6	0 %	1444	–
7	16 %	1297	Loose blend
8	16 %	1170	Randomly distributed pellets
9	32 %	1042	Loose blend
10	32 %	1129	Randomly distributed pellets
11	0 %	1490	Higher heat flux
12	0 %	1529	–
13	0 %	1557	–

Fig. 8. Comparison between a test without and with thermite, in the same wind tunnel conditions. a) On top, the reference run with the thin-walled BBU geometry (Test 4). b) Below, the same geometry with an internal charge of 58.2 g of thermite (Test 13).
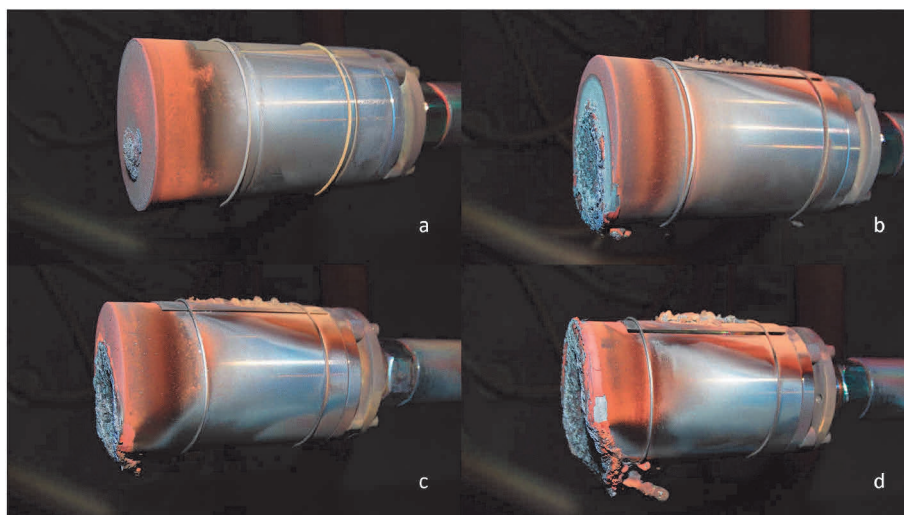

Fig. 9. Impact of an increasing charge of loose standard thermite on the demise of the thin-walled BBU sample. a) Reference test without thermite (Test 4). b) Test at 26 % filling (Test 6). c) Test at 39 % filling (Test 12). d) Test at 52 % filling (Test 13).
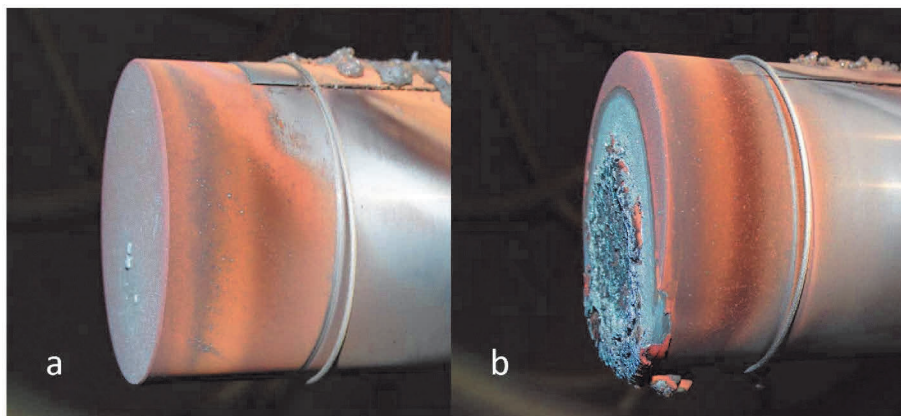
Fig. 10. Comparison between two tests of the thin-walled BBU in the same wind tunnel condition and with the same thermite mass, but with different blends granting different ignition temperature. a) On the left, run with lower temperature of ignition (Test 9). b) On the right, run with higher temperature of ignition (Test 6).

Table 4
Mass loss observed for three tests involving the thin-walled BBU at the same filling level, but with different charge compositions. "A″" and "P" stand respectively for loose and pelletized activated thermite dispersed in the main charge.

Test ID	Total mass of thermite [g]	Activated fraction [%w.t.]	Mass loss [g]
6	291	0	−6
9	289	32 (A)	−102
10	291	32 (P)	−57

typically implies partial oxidation of the aluminum powder: for this reason, the starting mixture is usually fuel rich to aim for stoichiometric conditions at the end of the production process. However, the fraction of active metal lost in this procedure is not easy to foresee. The thermite used in these tests was characterized through X-ray Diffraction Analysis (XRD), confirming an excess of fuel. For more detailed information, please refer to Ref. [40]. Another possibility is that the enthalpy released by the thermite was conducted away from the front face before the heat load from the wind tunnel could trigger its melting. Note that these effects could have acted synergistically, preventing the material from reaching the melting point.

The last major results of the experiments are related to the gas generation of the thermite charge. As discussed in Section 5.1.1, the loss of the lid in Tests 2 and 3 led to the addition of venting holes and to the run of the successive tests at lower filling. In the cases with venting holes, substantial gas and material ejection was observed. Furthermore, in some cases the reaction displayed an unsteady behavior shown in Fig. 11, which is still not explained.

5.2. Numerical results

In the following sections, the main computational results obtained with the modified version of SCARAB 3.1L WTM to account for the thermite thermal contribution are reported. The temperature of ignition of the thermite for each simulation was retrieved by the experimental data; therefore, the main parameters of merit to judge the adequateness of the numerical model are the ignition delay and the thermite-induced temperature jump (for tests without melting) or demise (for tests with melting). Please notice that the comparison between the experimental and numerical thermal traces is reported in Appendix A.

5.2.1. Ignition delay

In this work, the ignition delay is defined as the difference between the time needed to reach the ignition temperature in the simulations and the time needed to reach the ignition of the charge in the experiments,

after the exposure of the sample to the high-enthalpy flow. This value can be considered a parameter of merit to describe the adequateness of the model in representing the behavior of the system before the ignition. Indeed, the choice of using the experimental temperature of ignition as the trigger for the numerical reaction implies that the ignition delay is determined by the rebuilding of the temperature increase of the front face. In this description, an appropriate contact between the powder and the front face of the sample is assumed, as well as that the charge ignition is triggered in the proximity of the wall exposed to the flow. Table 5 reports the numerical and experimental ignition time for each test. It is evident that Tests 6 to 11 are well represented (ignition time lower than 20 s), while the other five tests report a substantial ignition delay.

When comparing Tables 3 and 5, a trend can be observed. The tests that show a significant ignition delay are characterized by both a high temperature of ignition and a high filling. An example is shown in Fig. 12a, where a comparison of the experimental and numerical temperature traces registered for the front face is reported. It is evident that up to 1200 K the experimental temperature evolution is well captured by the numerical model. At higher temperature, the experimental and numerical traces diverge. As the high ignition delays correlate with the high mass of thermite, a first explanation of this behavior could be the inadequateness of the thermite specific heat model explained in Section 4.2. To verify this hypothesis, additional simulations were performed without the thermite contribution to the overall specific heat of the system. An example of the results obtained is reported in Fig. 12b, where it is possible to see that the ignition delay decreases to 252 s for Test 2 (i. e., 14 s, or the 5 % of the starting ignition delay). Therefore, the thermite specific heat model seems not to be the main cause of this discrepancy. For this reason, all the simulations reported in Appendix A account for the thermite presence in the overall specific heat computation. Instead, it is hereby suggested that the insulating effect of the thermite, already observed in Section 5.1.1, plays a major role. A higher filling implies a higher insulating effect, especially at higher temperature, when internal radiation from the front face to the other internal surfaces becomes paramount. An experimental result indicating the importance of internal radiation for high temperature can be seen in Fig. 13, where the temperature of the front and rear walls before ignition for Tests 1, 5, and 2 are shown. These runs respectively involved the thick-walled geometry without charge, at 50 % filling, and at full filling. It is possible to see how, for high temperature, the temperature traces begin to diverge. Moreover, the rear thermocouple for the case without thermite registers a higher temperature. As the tests were conducted in near-vacuum condition, convection is expected to be negligible. Despite the potential partial detachment of the front thermocouple in the test without thermite, indicated by the irregular temperature profile, it is evident the
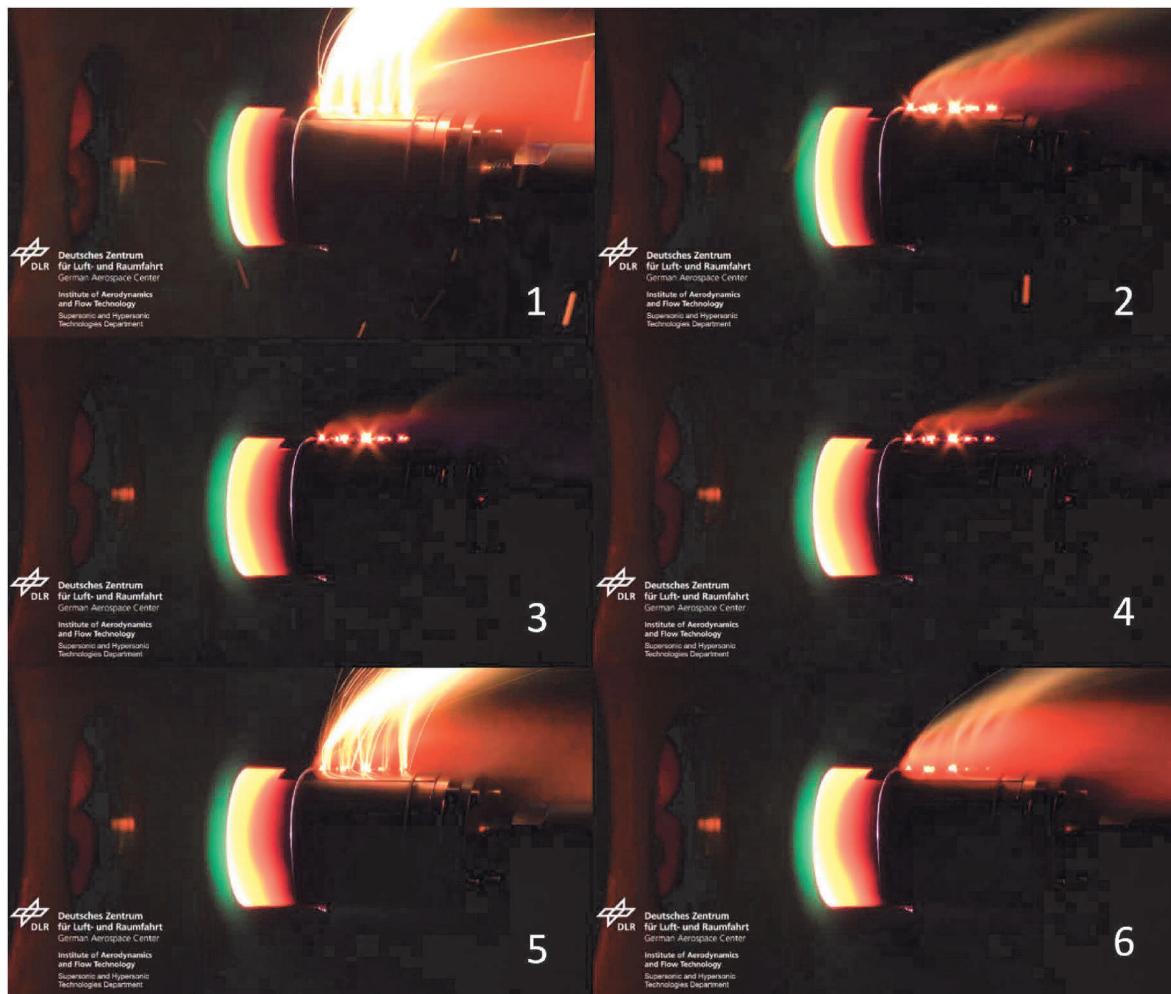
Fig. 11. Unsteady ejection from thin-walled BBU geometry, Test 12. Each frame is captured with a time interval of 0.2 s.

Table 5
Experimental and numerical ignition times for tests in which thermite was involved.

Test ID	Geometry and filling	Exp. Ignition time [s]	Num. Ignition time [s]	Ignition delay [s]
2	Thick-walled, 100 %	111	266	155
3	Thick-walled, 100 %	96	225	129
5	Thick-walled, 50 %	117	271	154
6	Thin-walled, 26 %	76	80	4
7	Thick-walled, 50 %	60	76	16
8	Thick-walled, 50 %	39	47	8
9	Thin-walled, 26 %	27	28	1
10	Thin-walled, 26 %	35	34	−1
11	Thin-walled, 26 %	72	83	11
12	Thin-walled, 39 %	73	125	52
13	Thin-walled, 52 %	74	125	51

importance of this insulating effect. This leads to a higher heating rate of the front face at high temperature in the experimental case, while currently in the numerical model this effect is not accounted for. In tests involving lower filling and activated thermite, the insulating effect of the internal charge is reduced and, therefore, the ignition is well captured.

5.2.2. Thermite-induced temperature increase

The effectiveness of the thermite in aiding the demise of the sample during the tests can be estimated by evaluating the thermite-induced temperature increases in the different runs. As the internal thermocouples are directly in contact with the pyrotechnic charge, it is not possible to consider them reliable anymore after the thermite ignition. For this reason, the temperature traces registered by the pyrometers are used for this evaluation. Please consider that the temperature data provided by the pyrometers is a local measurement.

Therefore, the comparison presented in this section between experimental and numerical data should be considered an estimate of the thermite influence on the system. It is possible that the gravity or the ejection of reacting material have determined a non-uniform heat transfer to the mock-up, which cannot be detected from the pyrometer signal. Please notice as well that as their signal was rather noisy, the values reported in Table 6 were determined graphically. Table 6 shows the comparison between experimental and numerical temperature increases that can be clearly identified after thermite ignition.

Tests 2, 3, 12, and 13 should be considered with caution. In particular, Tests 2 and 3 were the ones in which the lid was lost, implying the
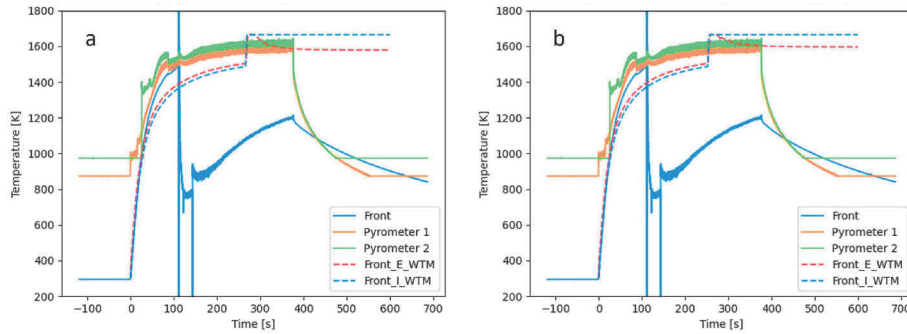
Fig. 12. Numerical rebuilding of Test 2, thick-walled BBU geometry at 100 % filling. a) On the left, thermite specific heat is accounted for, and numerical ignition takes place after 266 s. b) On the right, the thermite specific heat is not considered, and numerical ignition takes place after 252 s.
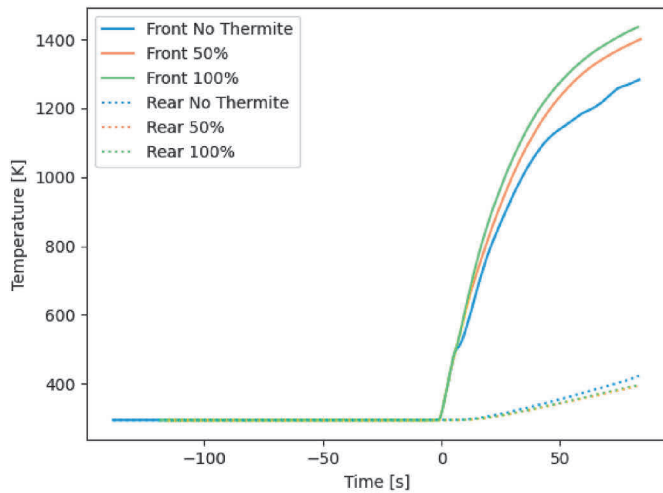
Fig. 13. Comparison between the front and rear face temperature traces in three conditions: no thermite, 50 % filling, and full filling. The Tests considered are respectively 1, 5, and 2.

Table 6
Approximated experimental and numerical thermite-induced temperature increase for tests in which thermite was involved. Please notice that P1 and P2 stand for the two different pyrometers, while the results obtained using a reaction duration of 4 s are marked with an asterisk (*).

Test ID	Exp. Temperature increase P1/P2 [K]	Num. Temperature increase [K]
2	25/25	175
3	25/25	180
5	240/190	175
6	195/165	180
7	160/180	225
8	65/55	305
9	100/140	290 (245*)
10	180/170	300 (280*)
11	220/170	155
12	285/225	125
13	400/245	125

ejection of almost all the thermite charge. This was verified checking the weight of the sample after the test and comparing it with the starting one. As no demise was detected, all weight loss corresponded to ejected thermite. This methodology determined that more than the 88 % of the initial charge was expelled, hence leading to the efficiency losses. In contrast, in Tests 12 and 13 effect of the thermite was substantial. The pyrotechnic charge provoked the partial melting of the front face, and this was correctly predicted by the numerical model. Therefore, the numerical thermite-induced temperature increase is limited to the

melting temperature of steel. This is the reason for the relatively low numerical temperature increase in these cases.

The rebuilding of Tests 5, 6, 7, and 11 is in very good agreement with experimental data, as the error with respect to the temperature data registered by the pyrometers is around 50 K or less. Test 8 involved multiple ignitions over a prolonged time span; therefore, it is complex to graphically quantify the effect of the thermite on the temperature trace. In contrast, in Tests 9 and 10 the time span in which the effect of the ignition on the temperature profile is experimentally registered is considerably shorter (about 4 s instead of 10 s). This is probably due to the increased fraction of activated thermite. For this reason, additional simulations were performed with a heat release duration of 4 s. The objective of these simulations is to verify whether the prolonged numerical heat release led to a fictitious increase in the final temperature jump as a result of the contribution of the head load from the WT. The results are shown in Table 6. Despite the decrease in the numerical temperature jumps, even the simulations with an enthalpy release duration of 4 s overestimate the temperature increase of the front face. It is suggested here that a significant portion of the reactive mixture was lost through the venting holes as a result of the higher pressure build-up created by the faster reaction. A detailed analysis of this phenomenon will be presented in further publications. Overall, the numerical model is able to foresee with adequate precision the effect of the thermite charge in case of uniform combustion of the internal mixture, if the internal pressure build-up is limited.

5.2.3. Shape of thermite-induced demised object

As reported in Section 5.2.2, for Tests 12 and 13, the increase in front face temperature is not an appropriate parameter for comparing experimental and numerical results. Indeed, as the sample reaches its melting point, the numerical temperature is upper-limited. Nevertheless, it is possible to compare the final geometry obtained in the numerical model and in the real tests. Fig. 14 shows a juxtaposition of recovered samples and numerical predictions. The dimension of the holes on the front face of the sample is well captured for both Test 12 and Test 13. An indicative quantification of the quality of the representation can be obtained by considering the equivalent diameter of the hole foreseen by SCARAB. Therefore, this diameter was computed as per Eq. (2).

$$d = 2\sqrt{\frac{\Delta m}{\pi \rho t}} \tag{2}$$

In Eq. (2), Δm is the mass lost during simulation, ρ is the steel 316L density (equal to 8000 kg/m₃), and t is the thickness of the front face, indicated in Fig. 2. Table 7 reports the comparison between the numerical and the experimentally measured breach diameter. It is important to notice that the experimental approximated value considers only the perforation and not the other damages that can be seen on the front face; therefore, a slight overestimation from the numerical model is
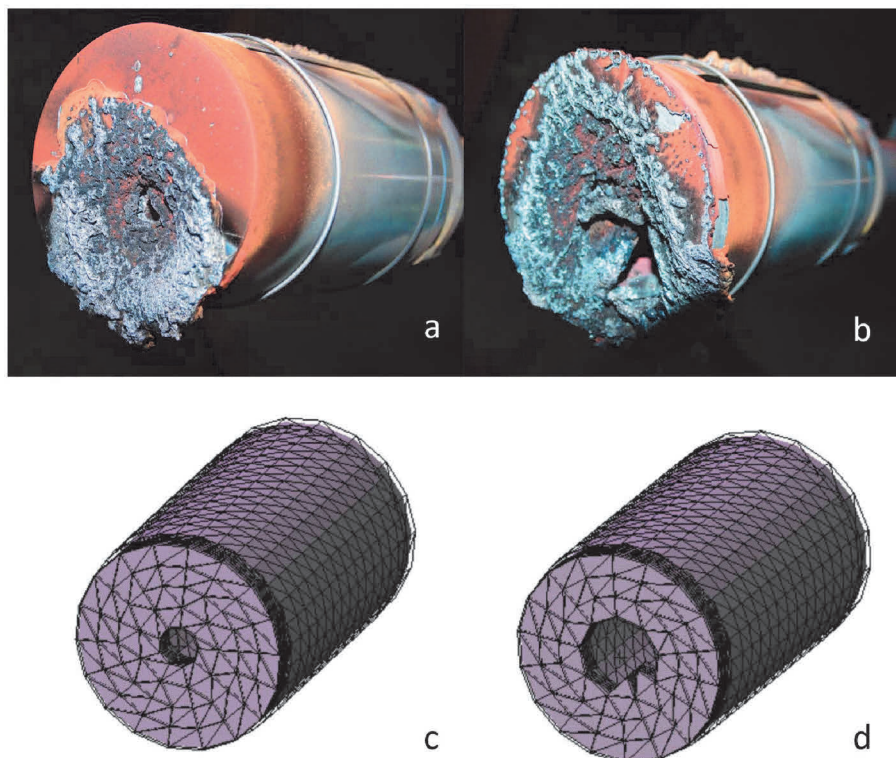
Fig. 14. Comparison between real samples after the experiments and numerical predictions (Tests 12 and 13). a) On the top left, the sample after Test 12. b) On the top right, the sample after Test 13. c) On the bottom left, predicted geometry for Test 12. d) On the bottom right, predicted geometry for Test 13.

Table 7
Comparison between the approximated experimental hole diameter and the numerical hole diameter prediction for Tests 12 and 13.

Test ID	Approx. exp. Hole diameter [mm]	Num. Hole diameter, d [mm]
12	12	16
13	21	24

reasonable. The simulations seem to adequately represent the overall demise.

A noticeable difference between the numerical and experimental final geometry is the position of the perforation for both the available cases. In the ground test, the presence of gravity and the absence of a tumbling motion caused the thermite to lie on the lower portion of the sample, leading to a hole that is not aligned with the sample axis. In predictions of the numerical package, developed to represent atmospheric re-entries, the hole is centered with respect to the sample geometry. This discrepancy is not expected in case of an actual re-entry application.

6. Conclusion

In this paper, the key results of the tests performed in the framework of the SPADEXO project on BBU-like geometries were presented. The results reported in this paper show that thermite-induced demise was effectively verified in a representative environment. Steel mock-ups were placed in the high-enthalpy hypersonic wind tunnel L2K, to investigate the effect of an internal thermite charge on the demise process under relevant conditions. Simple geometries were preferred to more complex shapes, with the goal of a simpler and more representative reconstruction in SCARAB. Different blends of standard and activated $Al + Fe_2O_3$ thermite were used, to control the passive ignition temperature of thermite. A new extension for SCARAB 3.1L was developed to rebuild the results of the activity. Thirteen test cases were

analyzed, focusing on the trends that could be observed during the experimental campaign. The thermite charge ignited reliably in all cases, and the dispersion of a mechanically activated fraction proved to be effective in controlling the temperature of ignition of the overall charge. A strong insulating effect of the mixture was observed. The numerical model showed good agreement with the experimental data in predicting the temperature increase of the front face as a result of the combustion of the thermite. Some intermittent reactions were observed experimentally, and it was not possible to rebuild their effect properly, because of the current definition of the numerical model, in which the reaction is assumed to take place in one single step. Partial demise was observed in some tests, while in the reference runs conducted in the same wind tunnel conditions but without the embedding of an internal thermite charge no demise took place. It was verified as well that the demise behavior is influenced by the thermite amount and its ignition temperature. In the cases in which the thermite reaction perforated the front face, SCARAB was able to replicate the damages that were observed on the mock-ups. The tests performed on the other geometry explored during the project (inspired by a Solar Array Drive Mechanism) as well as further analyses carried out on the BBU samples will be presented in further publications. The verified thermite-induced demise strongly encourages further research on this technology. Particular attention should be devoted to the gas generation properties of thermites to enable full filling tests in wind tunnels granting the safety of the facility. The development of numerical codes to describe the progress of the internal reaction and to estimate the pressure build-up inside a confined geometry is paramount. New concepts, beyond the simple direct integration inside the structural voids of components should be explored to investigate the capabilities of this new technology. Finally, tests on representative hardware could assess the real effectiveness of this strategy, once the numerical models will be validated on simple geometries.
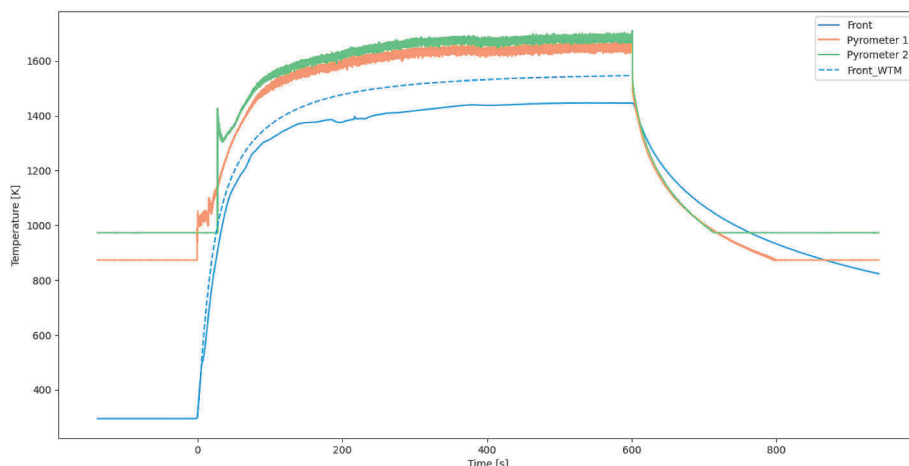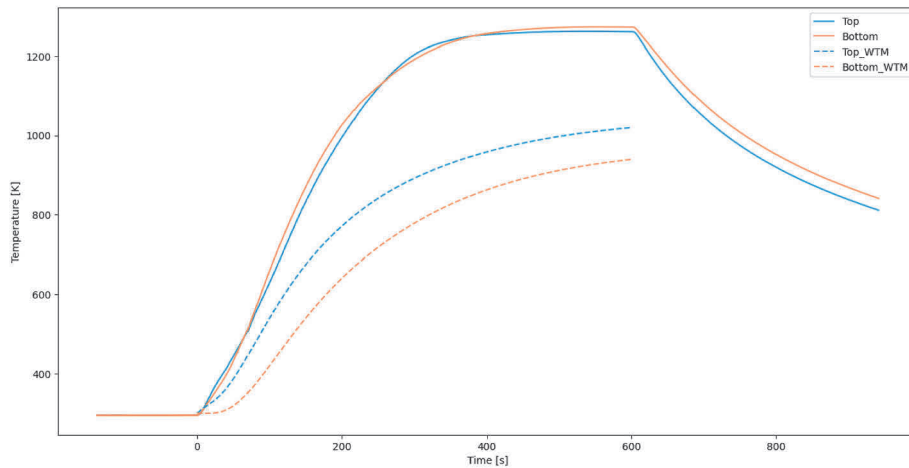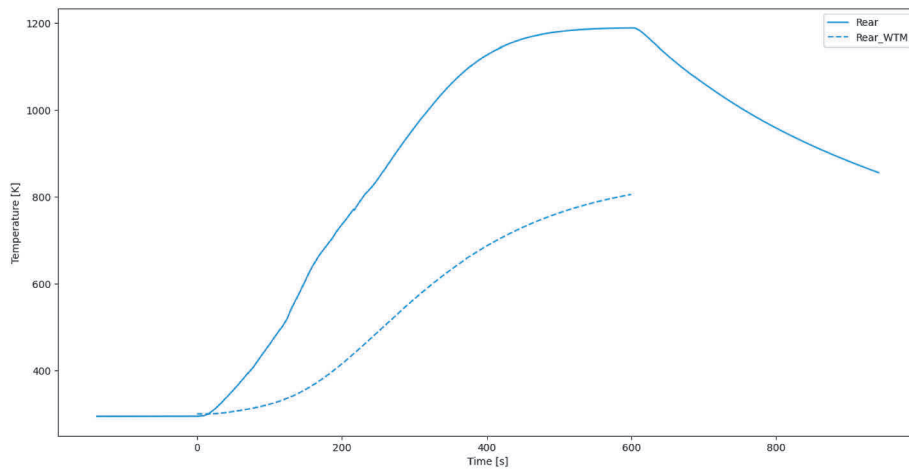
Fig. A1. Test 1. Thermal data obtained for thick-walled BBU geometry, no thermite charge, front face. Solid line is real acquisition, dashed line is numerical simulation.

CRediT authorship contribution statement

A. Finazzi: Conceptualization, Data curation, Formal analysis, Investigation, Methodology, Software, Validation, Writing – original draft, Writing – review & editing. **D. Daub:** Conceptualization, Data curation, Investigation, Methodology, Validation, Writing – review & editing. **F. Maggi:** Conceptualization, Investigation, Methodology, Supervision, Writing – review & editing. **C. Paravan:** Conceptualization, Writing – review & editing. **S. Dossi:** Conceptualization, Investigation, Methodology, Writing – review & editing. **T. Lips:** Conceptualization, Funding acquisition, Investigation, Methodology, Project administration, Software, Supervision, Writing – review & editing. **G. Smet:** Conceptualization, Supervision, Writing – review & editing. **K. Bodjona:** Conceptualization, Supervision, Writing – review & editing.

Declaration of competing interest

The authors declare the following financial interests/personal

relationships which may be considered as potential competing interests:

Filippo Maggi reports a relationship with ReActive Powder Technology s.r.l. that includes: board membership.

Stefano Dossi reports a relationship with ReActive Powder Technology s.r.l. that includes: board membership.

Tobias Lips reports financial support was provided by European Space Agency. Tobias Lips reports a relationship with HTG - Hyperschall Technologie Göttingen GmbH that includes: role as Managing Director.

Appendix A. Experimental and numerical temperature data

Appendix A.1 Nomeclature

Table A1 presents the abbreviations used in the legend of the data presented in Section Appendix A.2.

Table A1
Nomenclature used in the legend of the data presented in Appendix A.

Abbeviation	Description
WTM	Wind Tunnel Mode, numerical results
E	External
I	Internal

Appendix A.2. Data

Fig. A2. Test 1. Thermal data obtained for thick-walled BBU geometry, no thermite charge, top and bottom walls. Solid line is real acquisition, dashed line is numerical simulation.
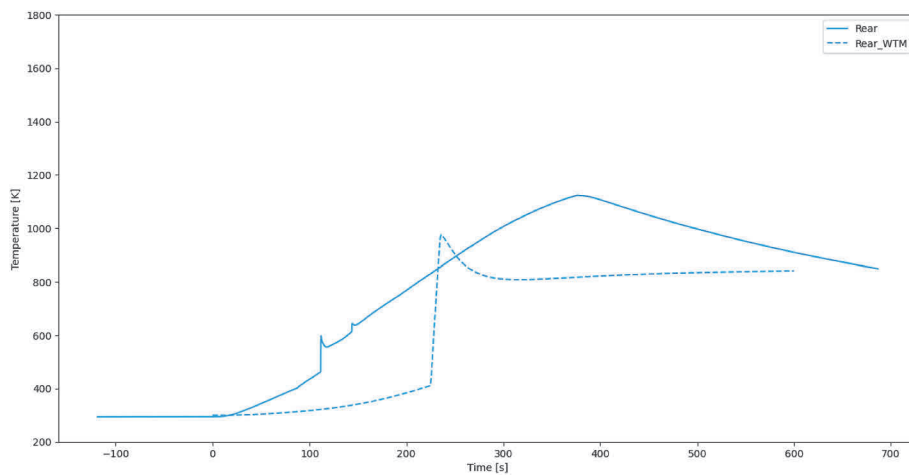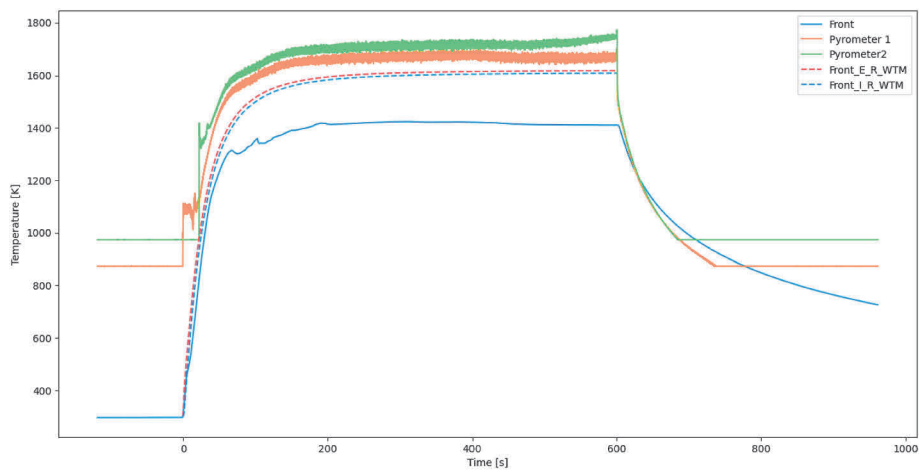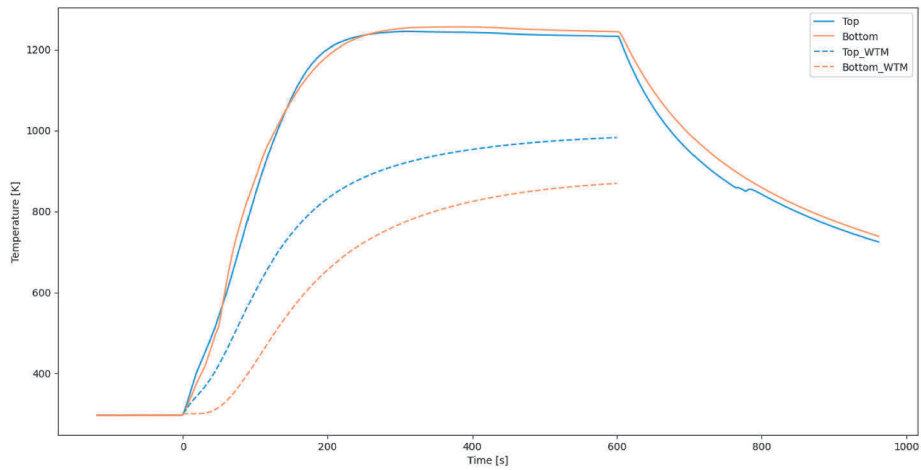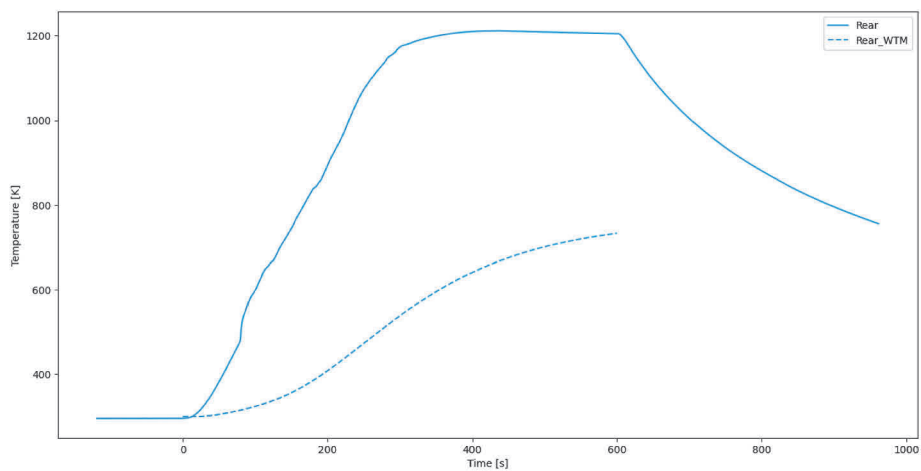

Fig. A3. Test 1. Thermal data obtained for thick-walled BBU geometry, no thermite charge, rear face. Solid line is real acquisition, dashed line is numerical simulation.
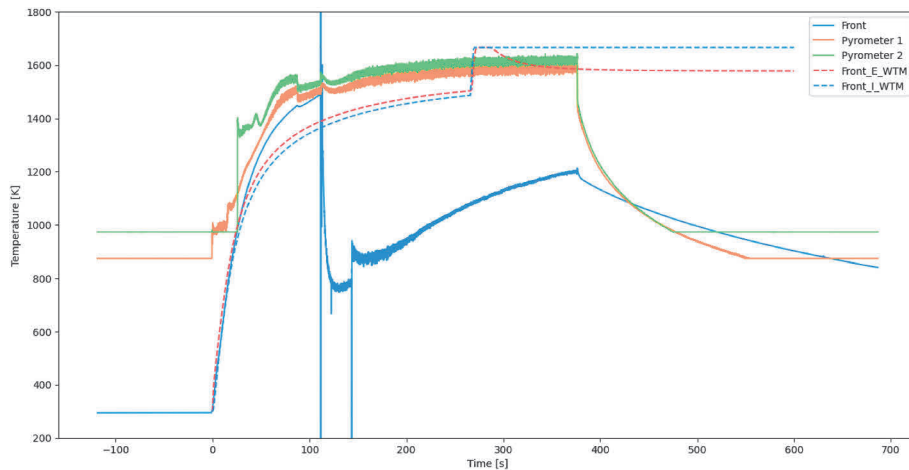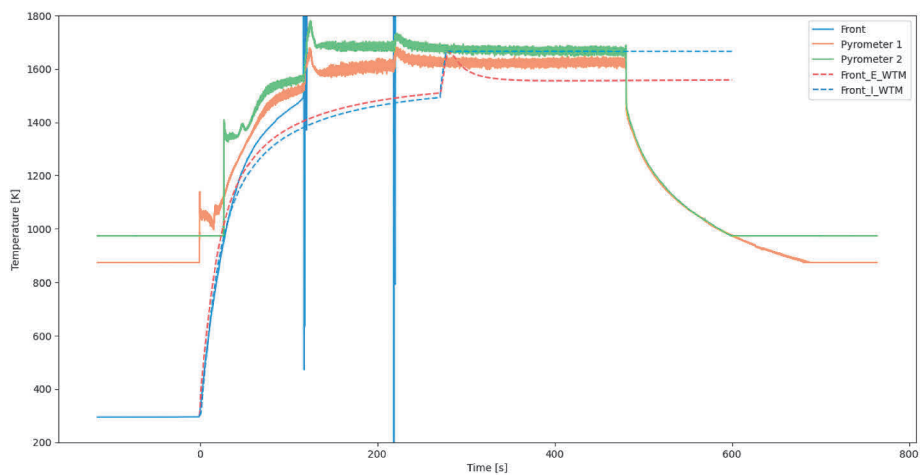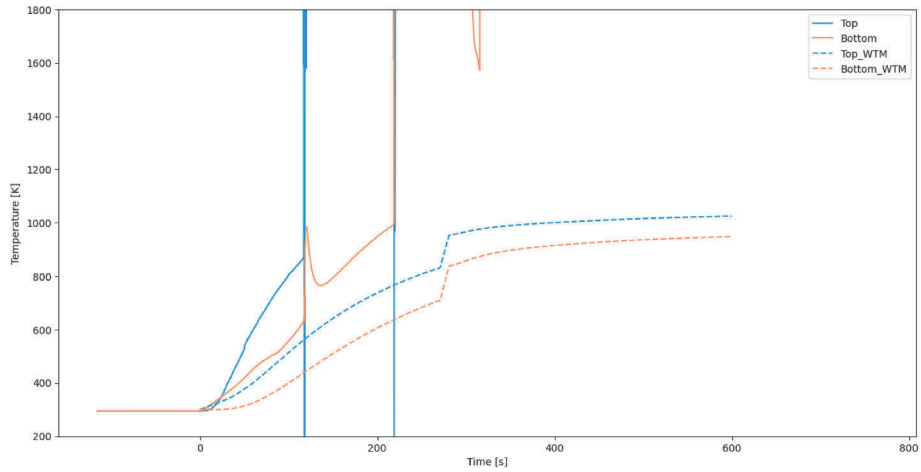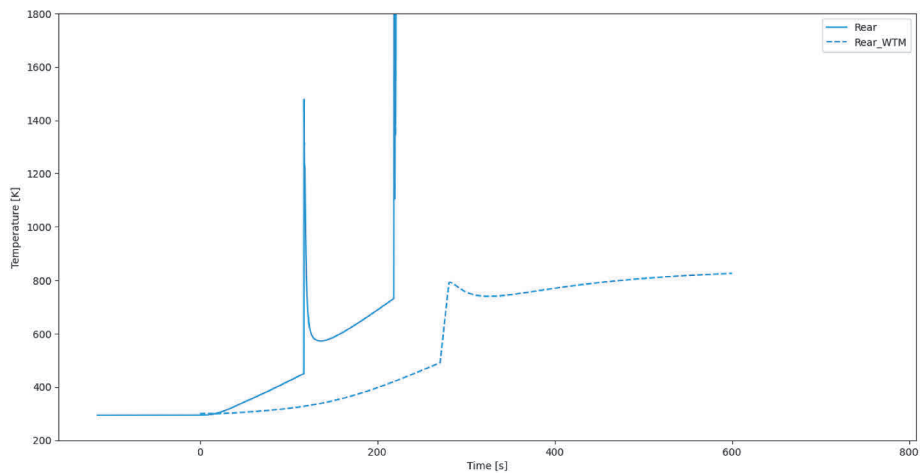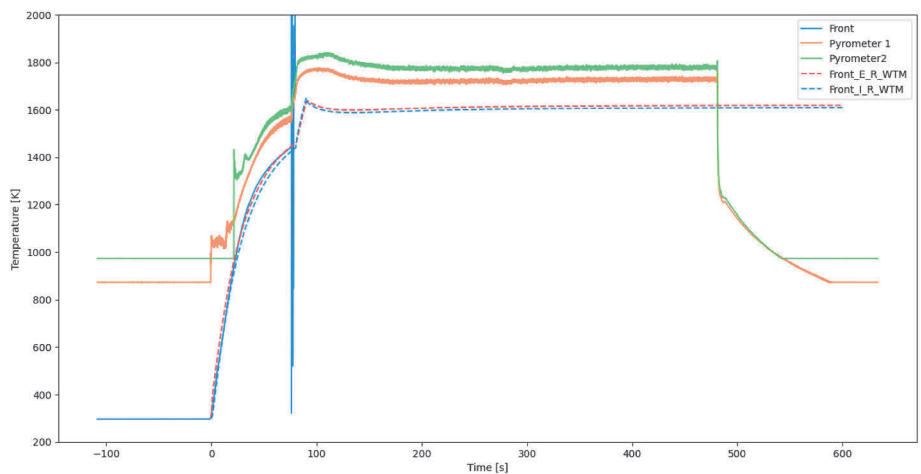

Fig. A4. Test 2. Thermal data obtained for thick-walled BBU geometry, full filling, front face. Solid line is real acquisition, dashed line is numerical simulation.
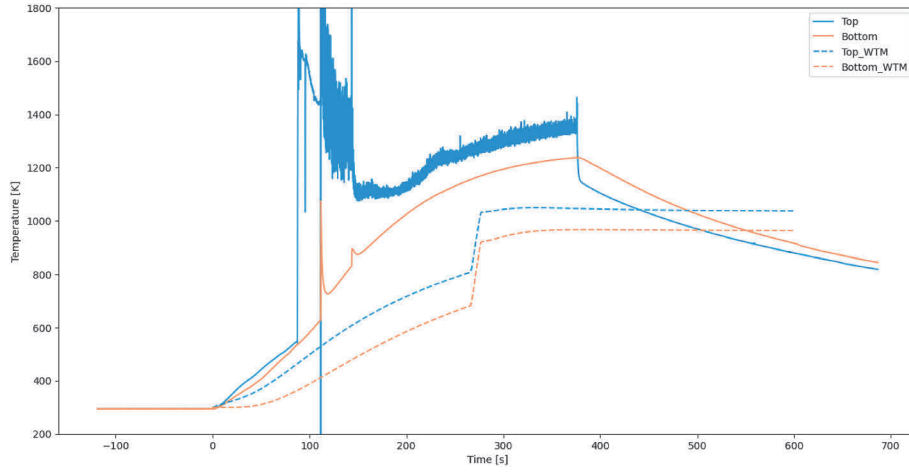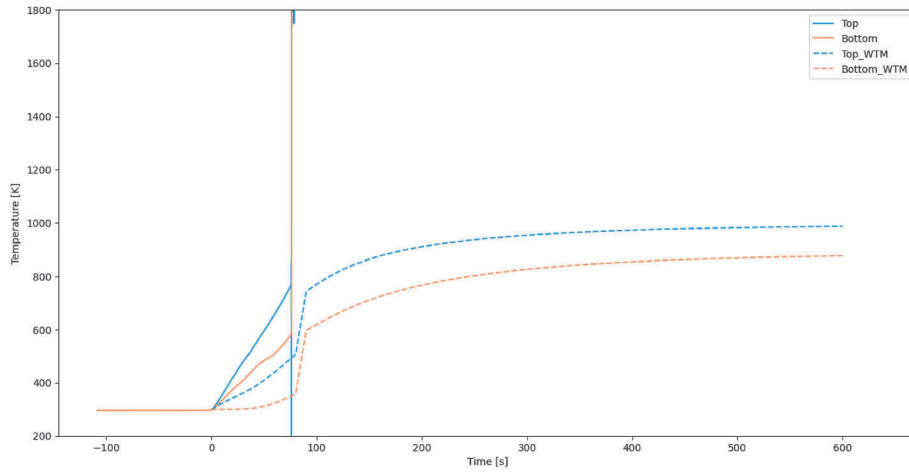
Fig. A5. Test 2. Thermal data obtained for thick-walled BBU geometry, full filling, top and bottom walls. Solid line is real acquisition, dashed line is numerical simulation.
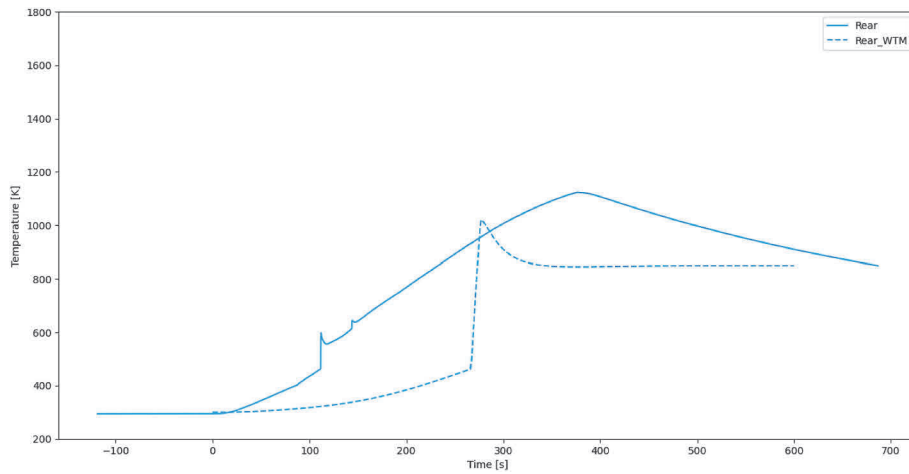
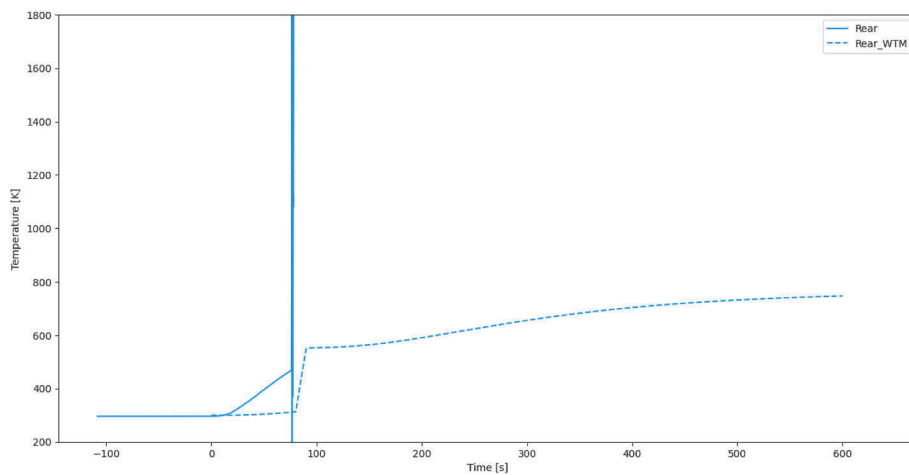**Fig. A6.** Test 2. Thermal data obtained for thick-walled BBU geometry, full filling, rear face. Solid line is real acquisition, dashed line is numerical simulation.
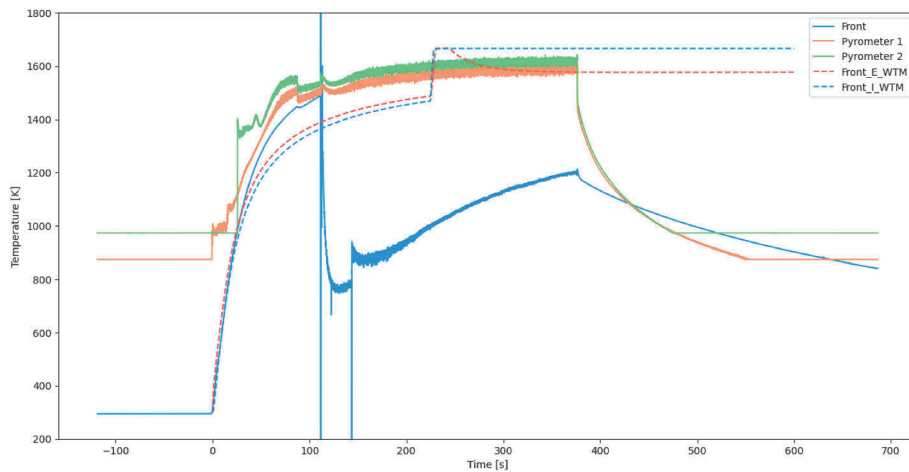
Fig. A7. Test 3. Thermal data obtained for thick-walled BBU geometry, full filling, front face. Solid line is real acquisition, dashed line is numerical simulation.
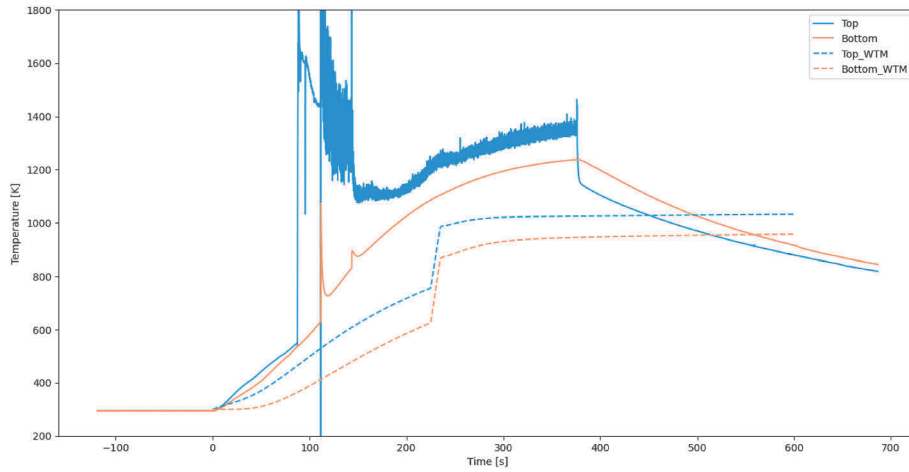
Fig. A8. Test 3. Thermal data obtained for thick-walled BBU geometry, full filling, top and bottom walls. Solid line is real acquisition, dashed line is numerical simulation.

Fig. A9. Test 3. Thermal data obtained for thick-walled BBU geometry, full filling, rear face. Solid line is real acquisition, dashed line is numerical simulation.

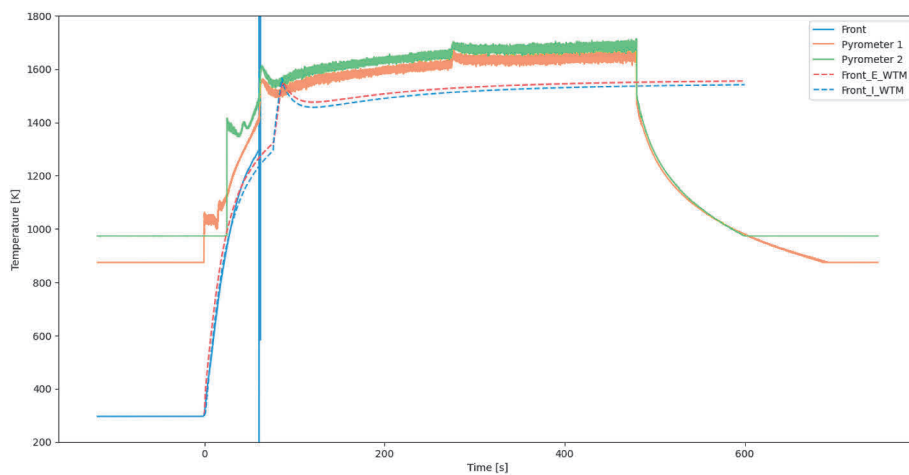**Fig. A10.** Test 4. Thermal data obtained for thin-walled BBU geometry, no thermite charge, front face. Solid line is real acquisition, dashed line is numerical simulation.

Fig. A11. Test 4. Thermal data obtained for thin-walled BBU geometry, no thermite charge, top and bottom walls. Solid line is real.

Fig. A12. Test 4. Thermal data obtained for thin-walled BBU geometry, no thermite charge, rear face. Solid line is real acquisition, dashed line is numerical simulation.

Fig. A13. Test 5. Thermal data obtained for thick-walled BBU geometry, 50 % filling, standard thermite, front face. Solid line is real.

Fig. A14. Test 5. Thermal data obtained for thick-walled BBU geometry, 50 % filling, standard thermite, top and bottom walls. Solid line is real acquisition, dashed line is numerical simulation.
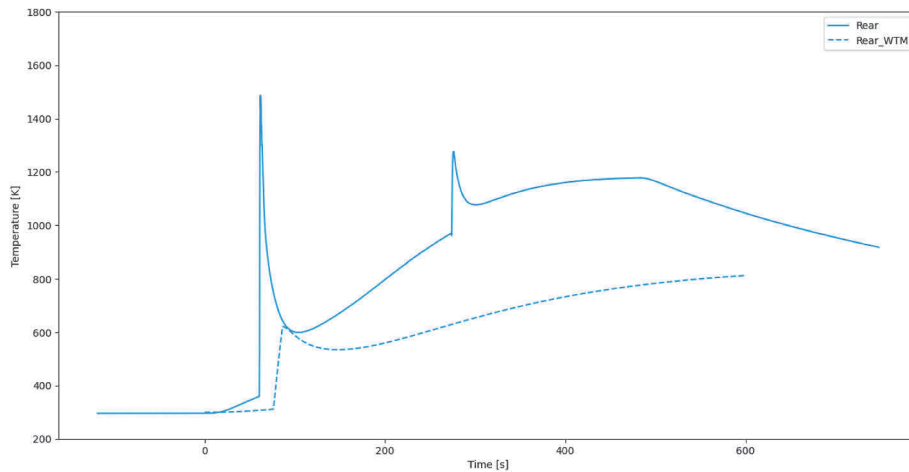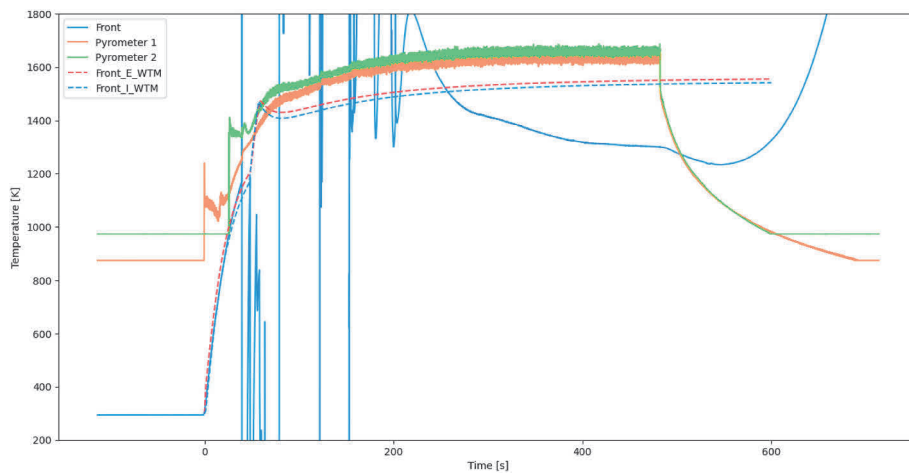

Fig. A15. Test 5. Thermal data obtained for thick-walled BBU geometry, 50 % filling, standard thermite, rear face. Solid line is real.

Fig. A16. Test 6. Thermal data obtained for thin-walled BBU geometry, 26 % filling, standard thermite, front face. Solid line is real acquisition, dashed line is numerical simulation.
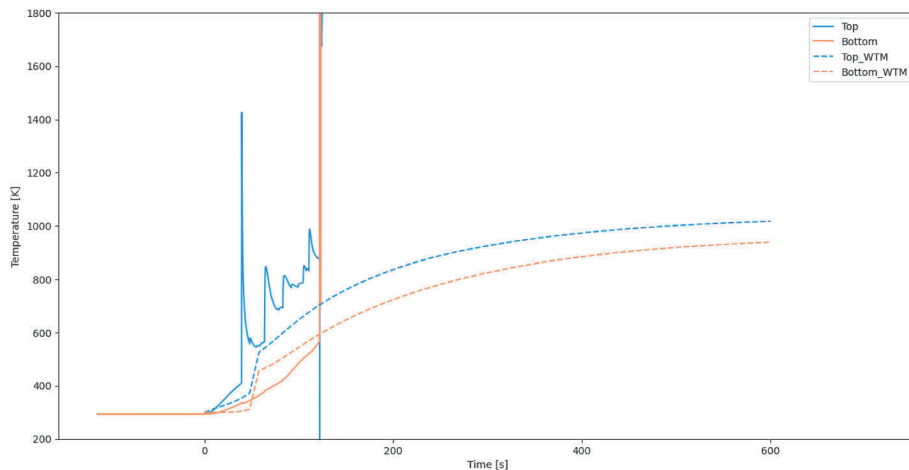
Fig. A17. Test 6. Thermal data obtained for thin-walled BBU geometry, 26 % filling, standard thermite, top and bottom walls. Solid line is real acquisition, dashed line is numerical simulation.

Fig. A18. Test 6. Thermal data obtained for thick-walled BBU geometry, 26 % filling, standard thermite, rear face. Solid line is real acquisition, dashed line is numerical simulation.

Fig. A19. Test 7. Thermal data obtained for thick-walled BBU geometry, 50 % filling, 16 % by mass activated loose thermite, front face. Solid line is real acquisition, dashed line is numerical simulation.
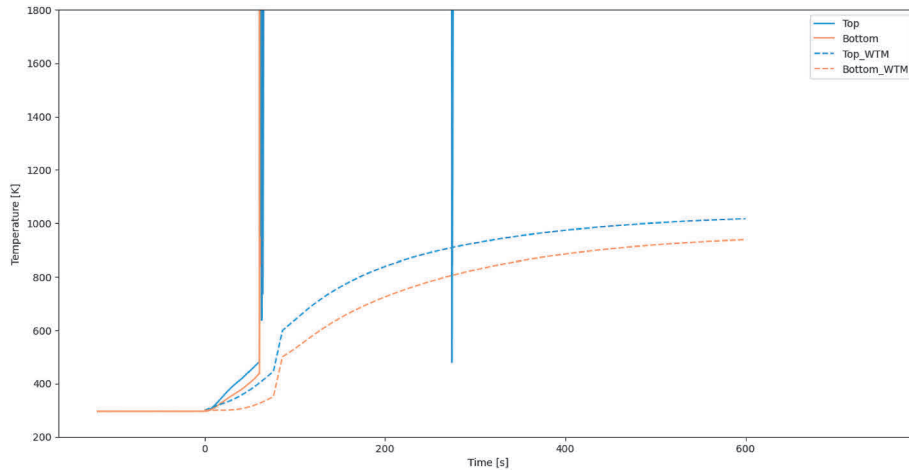
Fig. A20. Test 7. Thermal data obtained for thick-walled BBU geometry, 50 % filling, 16 % by mass activated loose thermite, top and bottom walls. Solid line is real acquisition, dashed line is numerical simulation.
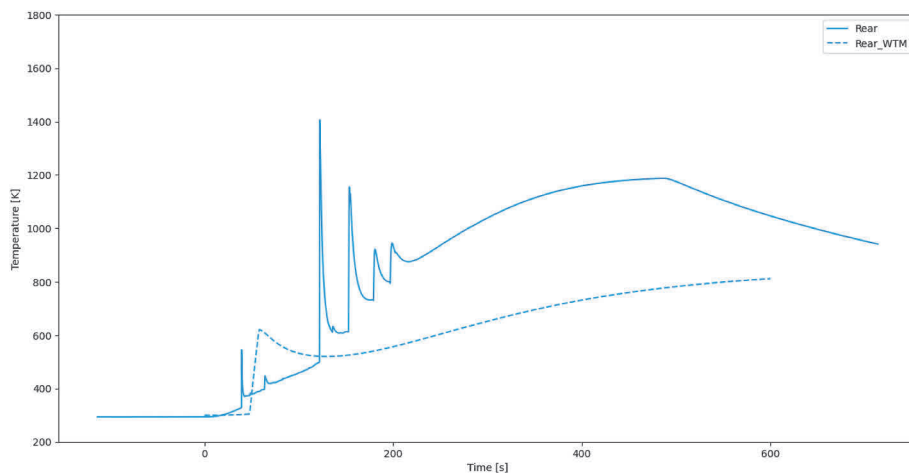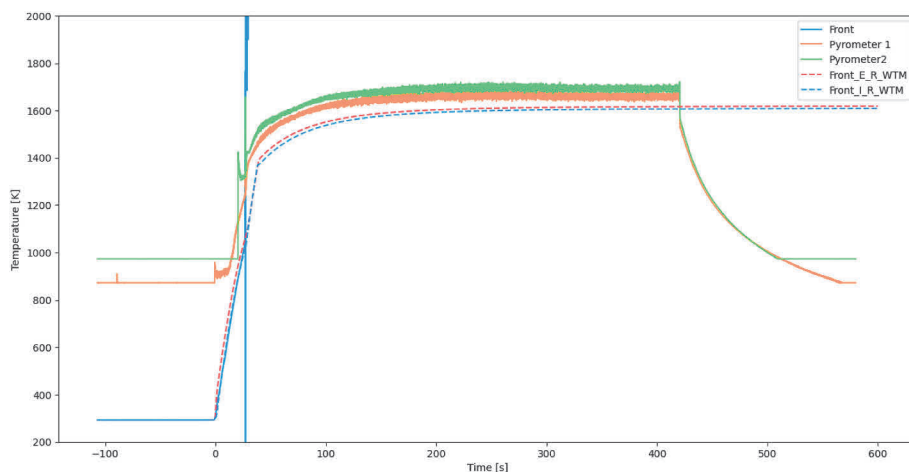

Fig. A21. Test 7. Thermal data obtained for thick-walled BBU geometry, 50 % filling, 16 % by mass activated loose thermite, rear face. Solid line is real acquisition, dashed line is numerical simulation.
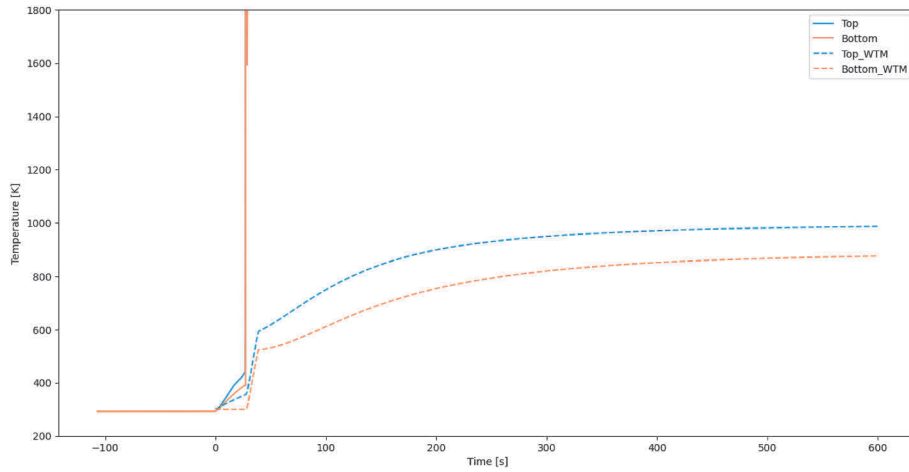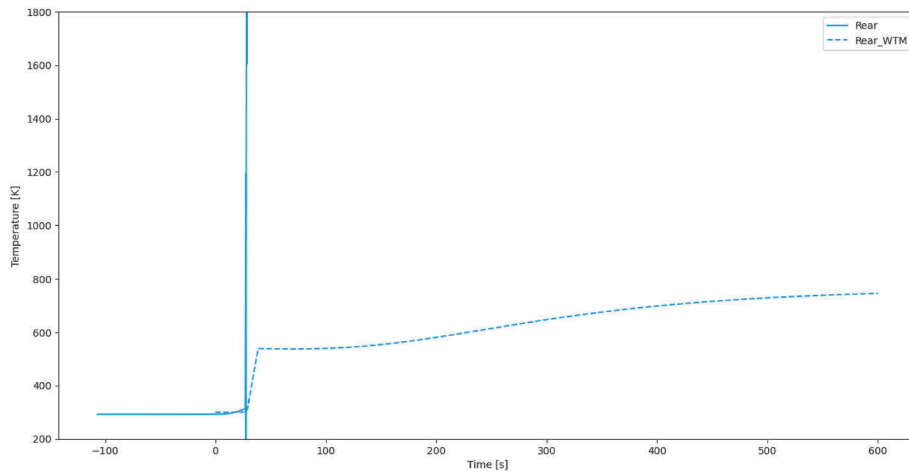

Fig. A22. Test 8. Thermal data obtained for thick-walled BBU geometry, 50 % filling, 16 % by mass activated pelletized thermite, front face. Solid line is real acquisition, dashed line is numerical simulation.

Fig. A23. Test 8. Thermal data obtained for thick-walled BBU geometry, 50 % filling, 16 % by mass activated pelletized thermite, top and bottom walls. Solid line is real acquisition, dashed line is numerical simulation.

Fig. A24. Test 8. Thermal data obtained for thick-walled BBU geometry, 50 % filling, 16 % by mass activated pelletized thermite, rear face. Solid line is real acquisition, dashed line is numerical simulation.

Fig. A25. Test 9. Thermal data obtained for thin-walled BBU geometry, 26 % filling, 32 % by mass activated loose thermite, front face. Solid line is real acquisition, dashed line is numerical simulation.
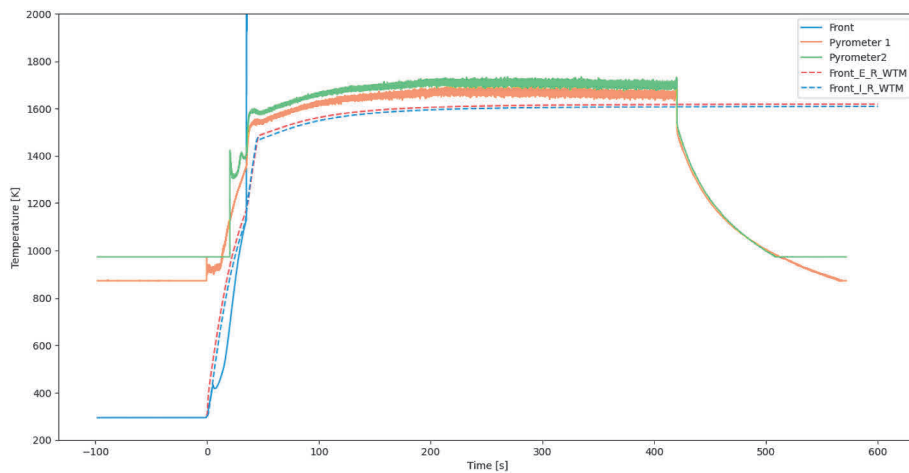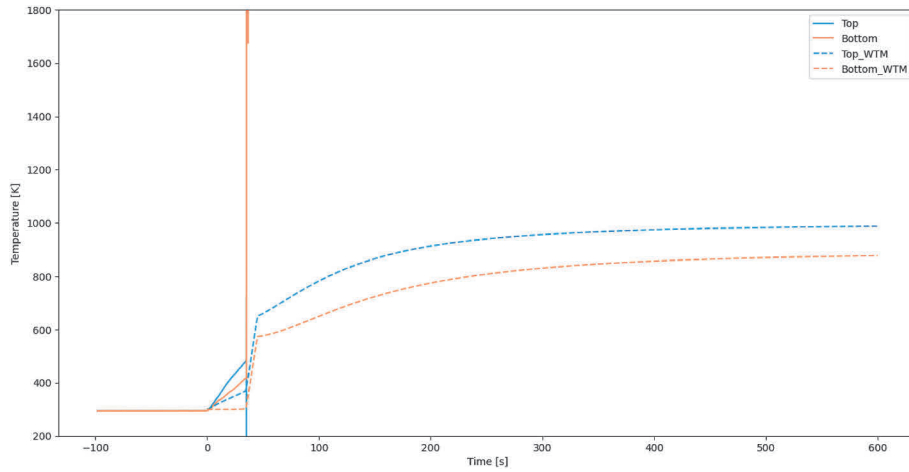
Fig. A26. Test 9. Thermal data obtained for thin-walled BBU geometry, 26 % filling, 32 % by mass activated loose thermite, top and bottom walls. Solid line is real acquisition, dashed line is numerical simulation.

Fig. A27. Test 9. Thermal data obtained for thin-walled BBU geometry, 26 % filling, 32 % by mass activated loose thermite, rear face. Solid line is real acquisition, dashed line is numerical simulation.

Fig. A28. Test 10. Thermal data obtained for thin-walled BBU geometry, 26 % filling, 32 % by mass activated pelletized thermite, front face. Solid line is real acquisition, dashed line is numerical simulation.

Fig. A29. Test 10. Thermal data obtained for thin-walled BBU geometry, 26 % filling, 32 % by mass activated pelletized thermite, top and bottom walls. Solid line is real acquisition, dashed line is numerical simulation.
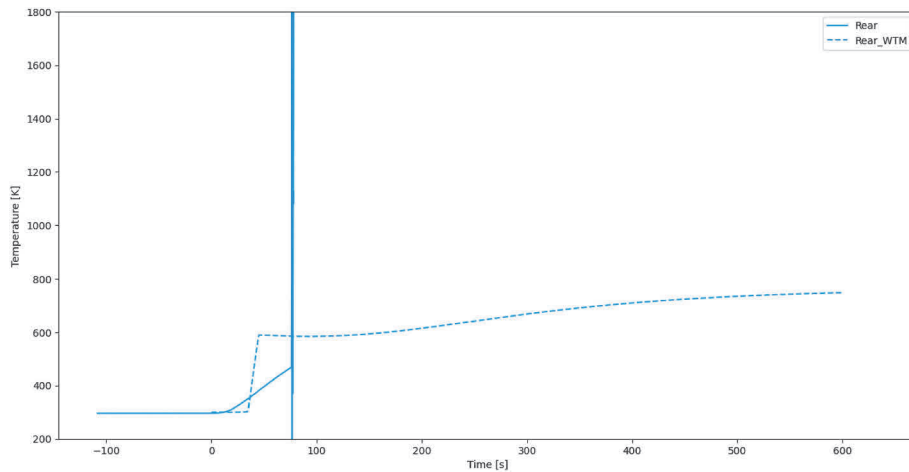

Fig. A30. Test 10. Thermal data obtained for thin-walled BBU geometry, 26 % filling, 32 % by mass activated pelletized thermite, rear face. Solid line is real acquisition, dashed line is numerical simulation.
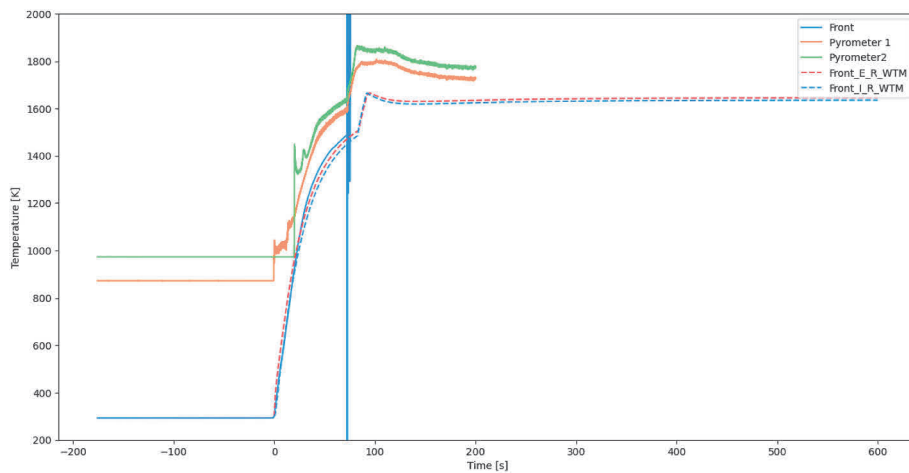

Fig. A31. Test 11. Thermal data obtained for thin-walled BBU geometry, 26 % filling, standard thermite, higher heat flux, front face. Solid line is real acquisition, dashed line is numerical simulation.
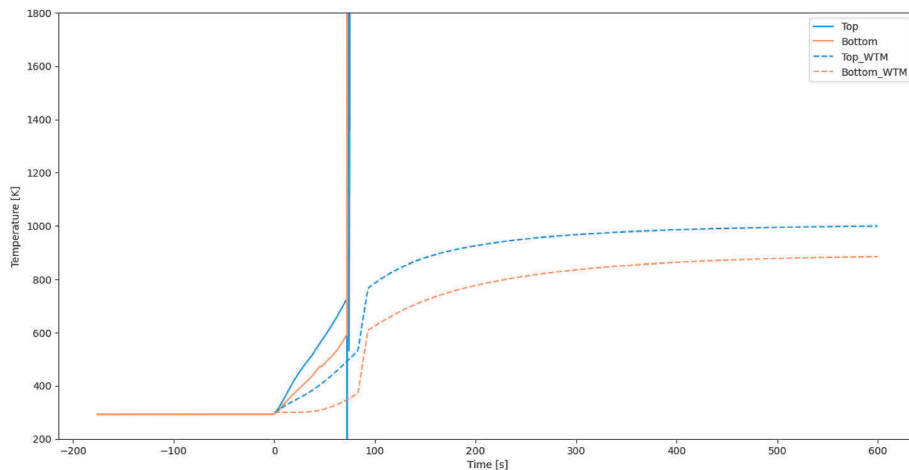
Fig. A32. Test 11. Thermal data obtained for thin-walled BBU geometry, 26 % filling, standard thermite, higher heat flux, top and bottom walls. Solid line is real acquisition, dashed line is numerical simulation.
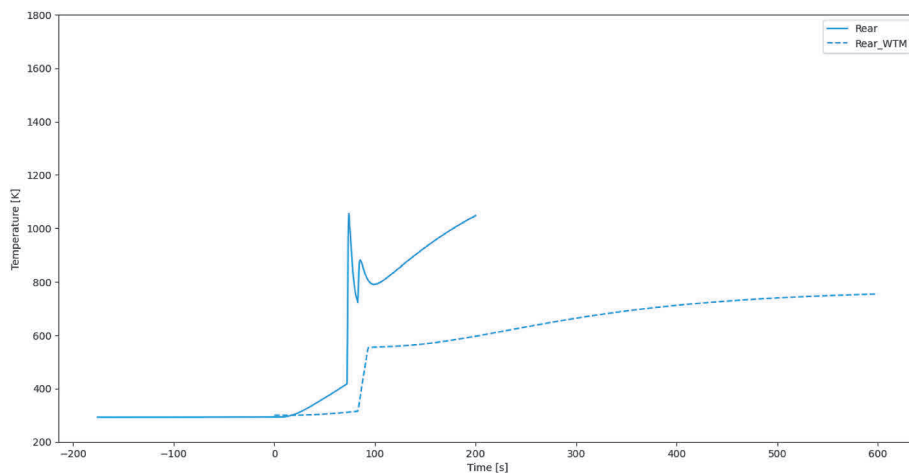

Fig. A33. Test 11. Thermal data obtained for thin-walled BBU geometry, 26 % filling, standard thermite, higher heat flux, rear face. Solid line is real acquisition, dashed line is numerical simulation.
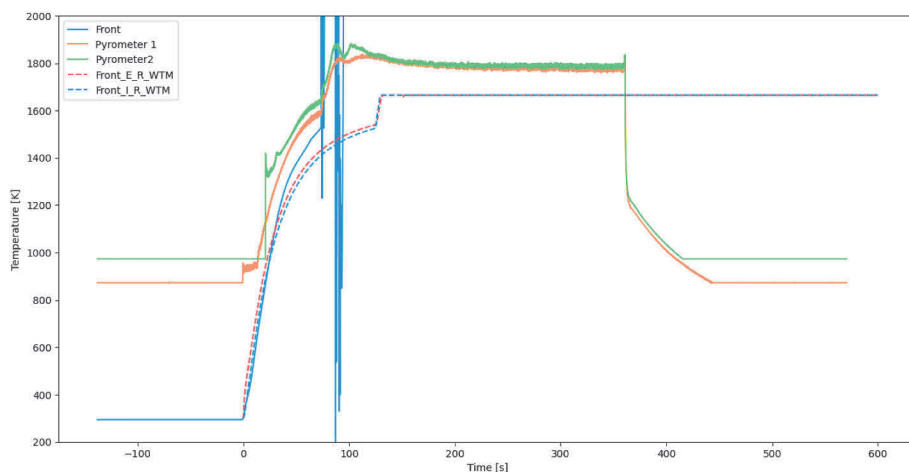

Fig. A34. Test 12. Thermal data obtained for thin-walled BBU geometry, 39 % filling, standard thermite, front face. Solid line is real acquisition, dashed line is numerical simulation.
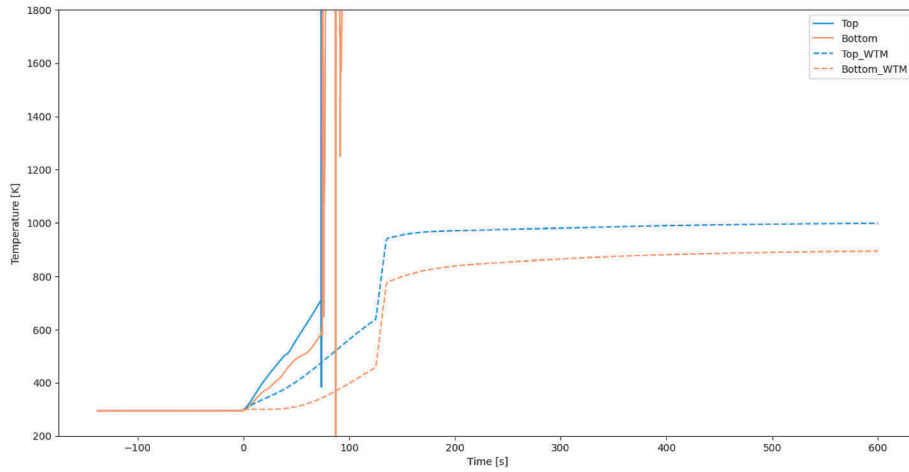
Fig. A35. Test 12. Thermal data obtained for thin-walled BBU geometry, 39 % filling, standard thermite, top and bottom walls. Solid line is real acquisition, dashed line is numerical simulation.
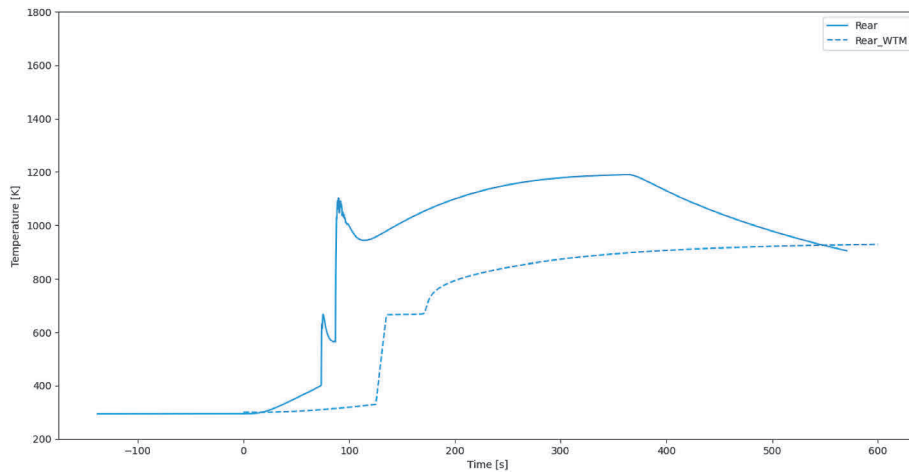

Fig. A36. Test 12. Thermal data obtained for thin-walled BBU geometry, 39 % filling, standard thermite, rear face. Solid line is real acquisition, dashed line is numerical simulation.

Fig. A37. Test 13. Thermal data obtained for thin-walled BBU geometry, 52 % filling, standard thermite, front face. Solid line is real acquisition, dashed line is numerical simulation.

Fig. A38. Test 13. Thermal data obtained for thin-walled BBU geometry, 52 % filling, standard thermite, top and bottom walls. Solid line is real acquisition, dashed line is numerical simulation.

Fig. A39. Test 13. Thermal data obtained for thin-walled BBU geometry, 52 % filling, standard thermite, rear face. Solid line is real acquisition, dashed line is numerical simulation.
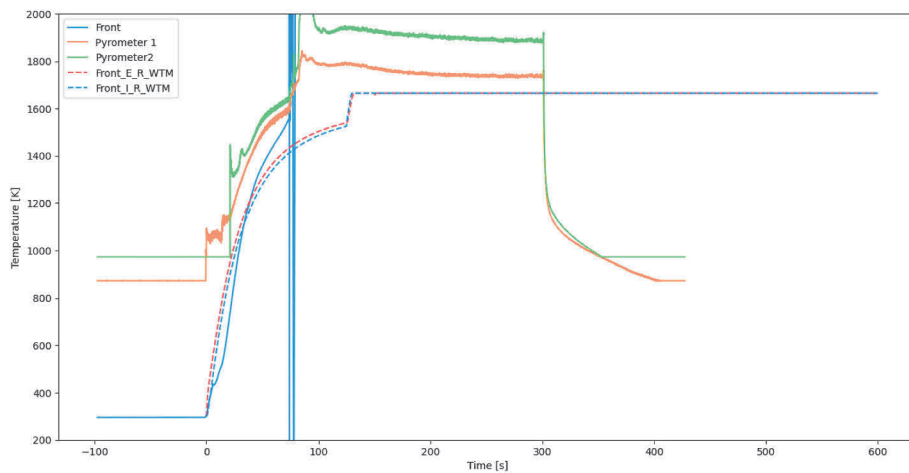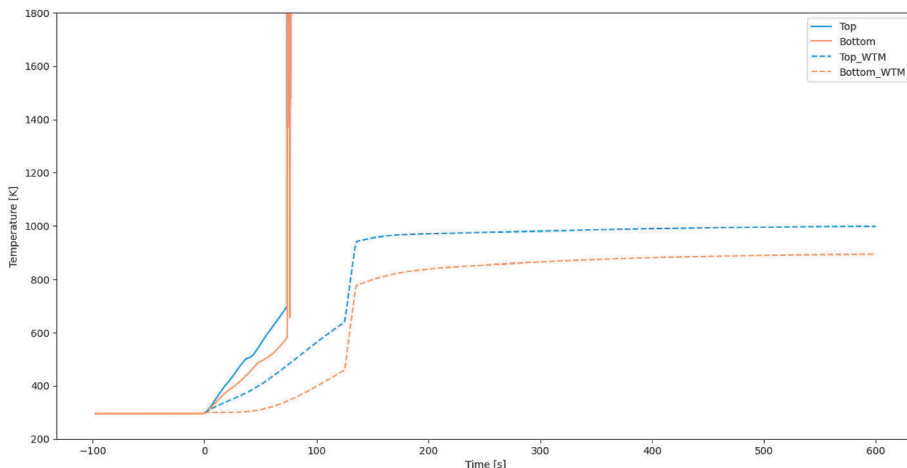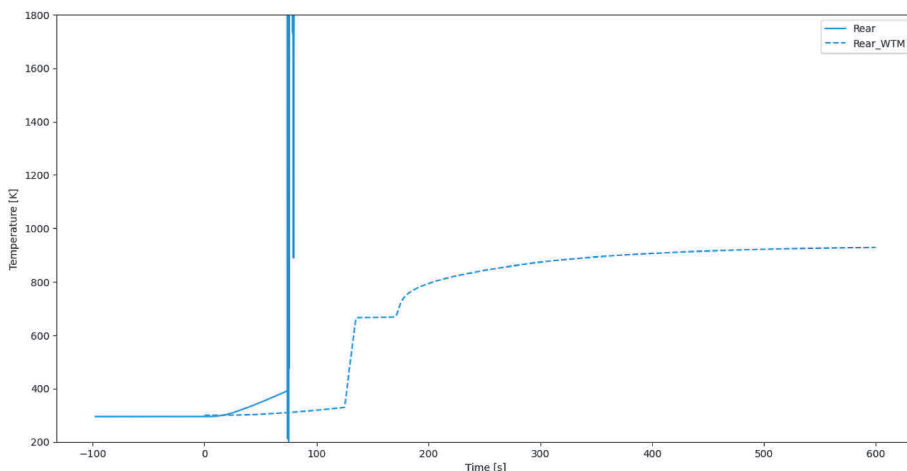
References

[1] Anon, World-first Zero Debris Charter Goes Live, European Space Agency, 2023. https://www.esa.int/Space_Safety/Clean_Space/World-first_Zero_Debris_Charter_goes_live. (Accessed 11 November 2023).
[2] Anon, Draft Council Conclusions on "Fair and Sustainable Use of Space, Council of European Union, 2023.
[3] Anon, Space innovation; mitigation of orbital debris in the new space age, FCC-Fact Sheet, Federal Communications Commission (2022) FCC-CIRC2209-01 available at: https://docs.fcc.gov/public/attachments/DOC-387024A1.pdf.
[4] AA. VV. ESA's Annual Space Environment Report, Issue 6, European Space Agency Space Debris Office, Darmstadt, Germany, 2022.
[5] AA. VV, *IADC Report on the Status of the Space Debris Environment*, Issue 1, Revision 0, Inter-Agency Space Debris Coordination Committee, 2020.
[6] AA. VV, *IADC Space Debris Mitigation Guidelines*, Revision 2, Inter-Agency Space Debris Coordination Committee, 2023.
[7] AA. VV, *Tri-Agency Reliability Engineering Guidance: Post Mission Disposal and Extension Assessment*, ESA-TECQQD-TN-025375/CAA-2021025/NASA SP-20210024973,ESA, JAXA, and NASA, (2022).
[8] ESA Director General's Office, Space Debris Mitigation Policy for Agency Projects, European Space Agency, Paris, ESA/ADMIN/IPOL(2014)2 , 2014.
[9] R. Kanzler, T. Lips, *Multi-Disciplinary Assessment of Design for Demise Techniques*, ESA CleanSpace Industrial Days, ESA/ESTEC, 2017.
[10] M. Trisolini. Space System Design for Demise and Survival, University of Southampton, Faculty of Engineering and the Environment, Department of Astronautics, 2018. PhD Thesis.
[11] D. Riley, I. Pontijas Fuentes, J. Meyer, G. Proffe, T. Lips, Design for Demise: systems-level techniques to reduce re-entry casualty risk, in: Proc. 7th European Conference on Space Debris, 2017. Paper No. 717.
[12] R. Seiler, G. Smet, Exothermic Reaction Aided Spacecraft Demise during, Re-entry, Patent EP3604143A1, 2018.
[13] D. Dihlan, P. Omaly, Élement de véhicule spatial a capacité d'autodestruction ameliorée et procedure de fabrication d'un tel élement, Patent FR 2975080B1, 2011.
[14] K.A. Monogarov, A.N. Pivkina, L.I. Grishin, YuV. Frolov, D. Dihlan, Uncontrolled re-entry of satellite parts after finishing their mission in LEO: titanium alloy degradation by thermite reaction energy, Acta Astronaut. 135 (2017) 69–75.
[15] S.H. Fischer, N.C. Grubelich, Theoretical Energy Release of Thermites, Intermetallics, and Combustible Metals, 24th International Pyrotechnics Seminar, Monterey, CA, 1998.
[16] Anon, ESA Space Debris Project – DRACO, European Space Agency, 2022 *[Online]*, https://www.esa.int/ESA_Multimedia/Images/2022/11/ESA_Space_Debris_project_-_DRACO. (Accessed 8 June 2023).
[17] R.G. Stern, Reentry Breakup and Survivability Characteristics of the Vehicle Atmospheric Survivability Project (VASP) Vehicles, The Aerospace Corporation, Report No TR-2008(8506)-3, (2008).
[18] AA. VV., Dive - guidelines for analysing and testing the demise of man made space objects during Re-entry. Technical Note ESA-TECSYE-TN-018311, European Space Agency, Noordwijk, The Netherlands, 2020.
[19] M.F. Campbell, T. Parise, A.M. Tulgestke, R.M. Spearrin, D.F. Davidson, R. K. Hanson, Strategies for obtaining long constant-pressure test times in shock tubes, Shock Waves 25 (2015) 651–665.
[20] C. Purpura, F. De Filippis, P. Barrera, D. Mandanici, Experimental characterisation of the CIRA plasma wind tunnel SCIROCCO test section, Acta Astronaut. 62 (2008) 410–421.
[21] AA. VV, Final Report - Upgrade of DRAMA's Spacecraft Entry Survival Analysis Codes, Hyperschall Technologie Göttingen GmbH, 2019. Contract No. 4000115057/15/D/SR, Issue 3, Revision 1.0.2.
[22] A. Finazzi, P. Finocchi, S. Carlotti, F. Maggi, Thermite-for-Demise (T4D): experimental analysis of heat transfer principles and preliminary sizing of an application, Int. J. Heat Mass Tran. 220 (2023) 124957, https://doi.org/10.1016/j.ijheatmasstransfer.2023.124957.

[23] Anon., European Space maTerIal deMisability dATabasE [Online], European Space Agency, https://estimate.sdo.esoc.esa.int/, Last access: 26/March/2024.

[24] J. Beck, I. Holbrough, J.A. Merrifield, N. Joiner, S. Bainbridge, Progress in hybrid Spacecraft/Object Oriented destructive re-entry modelling using the SAM code, in: Proc. 7th European Conference on Space Debris, 2017. Paper No. 415.

[25] M. Spel, J. Dumon, E. Constant, P. Van Hauwaert, S. Galera, J. Annaloro, Demisability study of industrial test cases with the Spacecraft-Oriented code PAMPERO, in: Proc. 8th European Conference on Space Debris (virtual), 2021. Paper No. 278.

[26] G. Koppenwallner, B. Fritsche, T. Lips, H. Klinkrad, Scarab - a multi-disciplinary code for destruction analysis of space-craft during re-entry. 5th European Symposium on Aerothermodynamics for Space Vehicles, 2005. Cologne, Germany.

[27] T. Schleutker, B. Esser, A. Gülhan, *Characterization of Demisable Materials (CHARDEM) – Final Report*, CHARDEM-DLR-TR3, DLR, Supersonic and Hypersonic Technologies Department, 2016. Cologne, Germany.

[28] B. Bonvoisin, M. Meisnar, J. Merrifield, J. Beck, T. Lips, A. Gülhan, T. Schleutker, G. Herdrich, A. Pagan, E. Kashnitz, V. Liedtke, B. Helber, S. Lopes, J.B. Gouriet, O. Chazot, T. Ghidini, Demisability assessment of space materials, CEAS Space Journal 15 (2023) 213–235.

[29] T. Schleutker, A. Gülhan, B. Esser, T. Lips, *ERASD – Exothermic Reaction Aided Spacecraft Demise – Proof of Concept Testing*, Test Report, DLR, Supersonic and Hypersonic Technologies Department, 2019. Cologne, Germany.

[30] M.J.M.M. Steenbergen, R.W. van Bezooijen, Rail welds, in: R. Lewis, U. Olofsson (Eds.), Wheel-rail Interface Handbook, Woodhead Publishing in Mechanical Engineering, Cambridge, UK, 2009.

[31] S. Turner, Thermite Cutting Device, Patent GB 2312864 A, 1997.

[32] J.C. Carter Jr., Portable Metal Cutting Pyrotechnic Torch, Patent US 2003/0145752 A1, 2003.

[33] S. Junghare, S. Kumari, A. Chaudhary, R. Kumar, S. Rayalu, Thermite reaction driven pyrotechnic formulation with promising functional performance and reduced emissions, J. Hazard Mater. 424 (2022) 127345.

[34] S. Kim, C. Schultz, C. Gotzmer, Incendiary Grenade, Patent US 9528803 B1, 2016.

[35] S. Dossi, C. Paravan, F. Maggi, L. Galfetti, Enhancing micrometric aluminum reactivity by mechanical activation, in: W. Pang, L. DeLuca, A. Gromov, A. Cumming (Eds.), Innovative Energetic Materials: Properties, Combustion Performance and Application, Springer, Singapore, 2020.

[36] C. Suryanarayana, Mechanical alloying and milling, Prog. Mater. Sci. 46 (2001) 1–184.

[37] A. Gülhan, B. Esser, Arc-heated facilities as a tool to study aerothermodynamic problems of reentry vehicles, in: D. Marren, F. Lu (Eds.), Advanced Hypersonic Test Facilities, Chapter 13, American Institute of Aeronautics and Astronautics, 2002, pp. 375–403.

[38] Anon., NIST-JANAF Tables [Online], National Institute of Standards and Technology, https://janaf.nist.gov/Last access: 26/March/2024.

[39] D. Daub, A. Finazzi, F. Maggi, T. Lips, P. Kärräng, *SPADEXO Test Report and Numerical Rebuilding*, Test Report WP 3210, WP 3310 (D7), DLR, Supersonic and Hypersonic Technologies Department, 2023. Cologne, Germany.

[40] A. Finazzi, S. Carlotti, C. Paravan, F. Maggi, S. Dossi, T. Lips, D. Daub, T. Schleutker, G. Smet, K. Bodjona, Thermite-for-Demise concept: from material selection to test campaign. 2024 AIAA Science and Technology Forum and Exposition, AIAA SciTech Forum), Orlando, FL, USA, 2024.